Soil Dynamics and Earthquake Engineering 92 (2017) 126–152

Contents lists available at ScienceDirect

Soil Dynamics and Earthquake Engineering

journal homepage: www.elsevier.com/locate/soildyn

Design of monopiles for offshore wind turbines in 10 steps

Laszlo Arany[a], S. Bhattacharya[b,*], John Macdonald[a], S.J. Hogan[a]

[a] University of Bristol, United Kingdom
[b] Chair in Geomechanics, University of Surrey, United Kingdom

ARTICLE INFO

Keywords:
Monopile
Offshore wind turbines
Eigen frequency
Design

ABSTRACT

A simplified design procedure for foundations of offshore wind turbines is often useful as it can provide the types and sizes of foundation required to carry out financial viability analysis of a project and can also be used for tender design. This paper presents a simplified way of carrying out the design of monopiles based on necessary data (i.e. the least amount of data), namely site characteristics (wind speed at reference height, wind turbulence intensity, water depth, wave height and wave period), turbine characteristics (rated power, rated wind speed, rotor diameter, cut-in and cut-out speed, mass of the rotor-nacelle-assembly) and ground profile (soil stiffness variation with depth and soil stiffness at one diameter depth). Other data that may be required for final detailed design are also discussed. A flowchart of the design process is also presented for visualisation of the rather complex multi-disciplinary analysis. Where possible, validation of the proposed method is carried out based on field data and references/guidance are also drawn from codes of practice and certification bodies. The calculation procedures that are required can be easily carried out either through a series of spreadsheets or simple hand calculations. An example problem emulating the design of foundations for London Array wind farm is taken to demonstrate the proposed calculation procedure. The data used for the calculations are obtained from publicly available sources and the example shows that the simplified method arrives at a similar foundation to the one actually used in the project.

1. Introduction

Offshore wind turbines are expected to operate for a lifetime of 20–30 years, while foundations are often designed for a longer design life. The selection of foundation type and the design is a complex task, which strongly depends not only on the site characteristics, but also on the maturity and track record of different design concepts. As the offshore wind industry is still in an early stage of large scale development, individual projects take a longer time than the rate at which technology advances. As such, it is not uncommon to change the type of turbine and the size/type of foundations during the development phase of a project. Therefore, development consent is typically obtained for a flexible project that allows for optimised detailed design using the most recent technological advances available at the time of final design. Consequently, it is important to have a simplified design procedure that allows for quick design using only limited site and turbine data, and that can be used in the tender design and early design phases of monopile foundations. Naturally, the procedure described in this paper has to be supplemented and refined with more accurate analyses when more information and data about the site conditions (met ocean data, geotechnical conditions) and chosen turbine becomes available. Accordingly, this paper does not aim to provide a methodology for detailed design and optimisation of monopiles but aims to provide a tool for initial design. Most importantly, the paper aims to show the multidisciplinary complex nature of the task. As such, the procedure defines the monopile through a simple geometry that is described by a pile diameter, wall thickness, pile length, and embedded length. Practical issues related to installation and manufacturing are discussed and it may be noted these aspects are beyond the scope of generalised simplified design procedure. However, it is suggested that manufacturing procedures can be taken into account through S-N curves required for typical welds.

One of the main aims of a foundation is to transfer all the loads from the wind turbine structure to the ground safely and within the allowable deformations. Guided by Limit State Design philosophy, the design considerations are to satisfy the following:

1. Ultimate Limit State (ULS): The first step in design is to estimate the maximum loads on the foundations (predominantly overturning moment, lateral load and the vertical load) due to all possible design load cases and compare with the capacity of the chosen foundation. For monopile type of foundations, this would require computation of

* Corresponding author.
E-mail addresses: S.Bhattacharya@surrey.ac.uk, Subhamoy.Bhattacharya@gmail.com (S. Bhattacharya).

http://dx.doi.org/10.1016/j.soildyn.2016.09.024
Received 6 November 2015; Received in revised form 18 September 2016; Accepted 19 September 2016
Available online 20 October 2016

Nomenclature

b_1, b_2	model parameters for Achmus et al. [4].
e	eccentricity of loading ($=M/F$)
f	zero shear force point location below mudline
f_0	first natural frequency
$f_{1P,max}$	upper limit of the 1P frequency range
f_{FB}	fixed base (cantilever beam) natural frequency of the tower
f_{yk}	characteristic yield strength
g	gravitational constant
g	distance from zero shear force location to pile toe
g_A	air gap between the highest expected wave crest level and the platform
k	wave number
k_0	equivalent stiffness of first tower mode
k_h	horizontal modulus of subgrade reaction
m	total structural mass, also strain accumulation exponent
m_0	equivalent mass of first tower mode
m_P	mass of the pile
m_{RNA}	mass of the rotor-nacelle assembly
m_T	mass of the tower
m_{TP}	mass of the transition piece
n_h	horizontal coefficient of subgrade reaction
n_{h1}	coefficient of subgrade reaction at the first load cycle
n_{hN}	coefficient of subgrade reaction after N load cycles
s	shape parameter of Weibull distribution
s_u	undrained shear strength of soil
t,t_a,t_b	time, also degradation parameters degradation model
t_G	grout thickness
t_P	pile wall thickness
t_T	tower wall thickness
t_{TP}	wall thickness of the transition piece
t_{TP}	transition piece wall thickness
u	turbulent wind speed component
u_{EOG}	extreme gust speed
$u_{EOG,U_{out}}$	Extreme Operating Gust (EOG) wind speed at cut-out wind speed
u_{ETM}	turbulent wind speed component for ETM
$w(x, z, t)$	horizontal water particle velocity
$\dot{w}(x, z, t)$	horizontal water particle acceleration
x_c	characteristics cyclic stress ratio
z_{hub}	hub height
A_R	Rotor swept area
C_L, C_R	lateral and rotational foundation flexibility coefficients
C_m	inertia coefficient
C_S	substructure flexibility coefficient
C_T	thrust coefficient
D	rotor diameter
D_b	bottom diameter of the tower
D_P	pile diameter
D_t	top diameter of the tower
D_{TP}	transition piece diameter
E_{eq}	equivalent Young's modulus
E_P	pile Young's modulus
$E_S(z)$	vertical distribution of soil's Young's modulus
E_{S0}	initial (small deformation) Young's modulus of soil at $1D_P$ depth
E_T	Young's modulus of the tower material
EI_η	equivalent bending stiffness for horizontal tower top loading
EOG	Extreme Operating Gust
ESS	Extreme Sea State
ETM	Extreme Turbulence Model
EWH	Extreme Wave Height
F_d	soil density parameter
F_f	horizontal load carrying capacity of the foundation
F_i	pile installation parameter
F_m	maximum horizontal force at the mudline expected in the lifetime of the turbine
F_r	cyclic load ratio parameter
F_{wave}	total horizontal wave force
$F_{wind,EOG}$	horizontal force due to the Extreme Operating Gust at rated wind speed
$F_{wind,ETM}$	horizontal force due to Extreme Turbulence Model at rated wind speed
F_x	fore-aft (along-wind) force on the turbine
F_D	drag force due to waves
F_I	inertia force due to waves
F_R	horizontal load capacity of the foundation (assuming soil failure)
FLS	Fatigue Limit State
G^*	modified shear modulus
G_S	soil's shear modulus
H_m	maximum wave height (for a given significant wave height H_S)
$H_{m,50}$	maximum wave height expected in 50 years
H_S	significant wave height
$H_{S,50}$	50-year significant wave height
HWL	Highest Water Level with 50 year return period
I	reference turbulence intensity
I_P	pile's second moment of area
I_T	second moment of area of tower
K	scale parameter of Weibull distribution
K_L	lateral stiffness of the foundation
K_{LR}	cross coupling stiffness of the foundation
K_P	Rankine coefficient of passive pressure
K_R	rotational stiffness of the foundation
L_k	horizontal turbulence integral length scale
L_P	pile embedded length
L_S	platform height (distance from mudline to platform level, that is to the top of the transition piece)
L_T	tower length
L_{TP}	length of the transition piece
M_{amp}	amplitude of the bending moment in a load cycle ($=M_{max}-M_{min}$)
M_f	overturning moment capacity of the foundation
M_{ULS}	maximum overturning moment at the mudline expected in the lifetime of the turbine
M_{max}	maximum bending moment in a load cycle
M_{mean}	mean bending moment in a load cycle ($=0.5\bullet(M_{max}+M_{min})$)
M_{min}	minimum bending moment in a load cycle
M_y	fore-aft (along-wind) overturning moment
M_R	overturning moment capacity of the foundation (assuming soil failure)
M_{wave}	total overturning moment due to waves
$M_{wave,NWH}$	total overturning moment due to waves for normal wave height (NWH)
$M_{wave,EWH}$	total overturning moment due to waves for extreme wave height (EWH)
$M_{wind,EOG}$	overturning moment due to the Extreme Operating Gust at rated wind speed
$M_{wind,ETM}$	overturning moment due to Extreme Turbulence Model at rated wind speed
N	number of load cycles
NSS	Normal Sea State
NTM	Normal Turbulence Model
NWH	Normal Wave Height

P_R	rated power
R_d	relative density
R_L	length to diameter ratio of the pile
S	maximum water depth
$S_{uu}(f)$	Kaimal wind spectrum
SLS	Serviceability Limit State
SSS	Severe Sea State
$T_b(\zeta_b,\ R_d)$	tilt accumulation magnitude function
$T_c(\zeta_c)$	tilt accumulation load characteristics function
T_L	expected lifetime of the foundation
T_S	time period of waves
Th	Thrust force on the rotor
Th_{mean}	Mean thrust force
Th_{turb}	Turbulent thrust force
U	Wind speed at hub height
$\overline{U}$	Mean wind speed
$U_{10,50-year}$	50 year maximum 10-min mean wind speed
$U_{10,1-year}$	1-year maximum 10-min mean wind speed
U_{in}	cut-in wind speed
U_{out}	cut-out wind speed
U_R	rated wind speed
ULS	Ultimate Limit State
V	vertical load (force)
V_f	vertical load carrying capacity of the foundation
V_m	maximum vertical force on the foundation
γ	specific weight
γ'	submerged unit weight of soil
γ_L	load factor
γ_M	material factor
ε_1	strain at first load cycle
ε_N	accumulated strain after N load cycles
ε_p	plastic strain
ζ_b	load magnitude parameters
ζ_c	cyclic load parameter
$\eta(x,\ t)$	wave elevation
η_{50}	50-year maximum wave crest
η_L	non-dimensional lateral stiffness
η_{LR}	non-dimensional cross coupling stiffness
η_R	non-dimensional rotational foundation stiffness
θ	pile rotation
θ_0	mudline rotation at first load cycle at mudline
θ_{acc}	accumulated rotation at the mudline
θ_N	mudline tilt after N load cycles
θ_S	mudline rotation due to static loading
$\Lambda_1=L_k/8$	integral length scale parameter
ν_S	soil's Poisson's ratio
ρ	pile deflection
ρ_0	initial deflection at the mudline
ρ_{acc}	accumulated deflection at the mudline
ρ_a	Air density
ρ_P	density of the pile material
ρ_T	density of the tower material
ρ_{TP}	density of the transition piece material
ρ_w	density of sea water
σ_c	cyclic stress amplitude
σ_{end}	endurance limit of pile steel
σ_m	maximum stress level
$\sigma_{U,c}$	characteristic standard deviation of wind speed
$\sigma_{U,f>1P}$	standard deviation of turbulence above $f_{1P,max}$
$\sigma_{U,ETM}$	Extreme Turbulence Model wind speed standard deviation
ϕ	angle of wind-wave misalignment
ϕ'	friction angle of the soil
Φ	Cumulative Distribution Function
Φ_{U10}	Cumulative Distribution Function of 10-min mean wind speeds
$\Phi_{U10,1-year}$	Cumulative Distribution Function of yearly maximum 10-min mean wind speeds
χ	bending stiffness ratio ($E_T I_T/E_P I_P$)
ψ	length ratio of platform height and tower height (L_S/L_T)
ω	circular frequency of waves
Ω	rotational speed of the turbine rotor

ultimate moment, lateral and axial load carrying capacity. Therefore inevitably, ULS design consideration will provide the minimum dimension (length and diameter) of the monopile and also the wall thickness required. The input required for such calculations are site characteristics (for example wind and wave data) and turbine data. The load calculation procedure is described in Section 2.2. At some sites, some other loads (for example ice load or earthquake loads) may need to be considered.

2. Target Natural Frequency (Eigen frequency) and Serviceability Limit State (SLS): This requires the prediction of the natural frequency of the whole system (Eigen frequency) and the deformation of the foundation at the mudline level (which can be further extrapolated to the hub level) over the life time of the wind turbine. As natural frequency is concerned with very small amplitude vibrations (linear Eigen Value Analysis will suffice) the deformation of the foundation will be small and prediction of initial foundation stiffness would suffice for this purpose. Therefore the second major calculation is the determination of stiffness of the foundation (covered in Section 2.4) whereby a closed form solution is presented to obtain the foundation stiffness for rigid monopiles as well as flexible monopiles. These foundation stiffness values can be used to estimate the deformation (pile head rotation and displacement) and natural frequency of the whole system. In Section 2.6, a closed form solution is presented to obtain the natural frequency of a wind turbine taking into consideration the flexibility of the foundation and substructure.
3. Fatigue Limit State (FLS) and long term deformation: This would require predicting the fatigue life of the monopile as well as the effects of long term cyclic loading on the foundation.
4. Robustness and ease of installation: This step will ascertain that the foundation can be installed and that there is adequate redundancy in the system.

The SLS and ULS modes of failure are schematically described in Fig. 1. ULS failure (which can also be described as collapse) can be of two types: (a) where the soil fails; (b) where the pile fails by forming a plastic hinge. On the other hand, in SLS failure, the deformation will exceed the allowable limits. Other design issues can be found in Bhattacharya [15].

The foundation design procedure compliant with the current codes of practice can be summarized in the following 10 major steps. The interdependency of design steps and necessary inputs for all steps are shown in Fig. 2. The order of the suggested calculation steps are shown below:

(1) Establish design basis (design criteria: ULS, FLS, SLS) and collect input data (turbine, metocean and geotechnical data) where some of the criteria may be project or country specific.
(2) Guess initial pile dimensions based on wind load estimation and

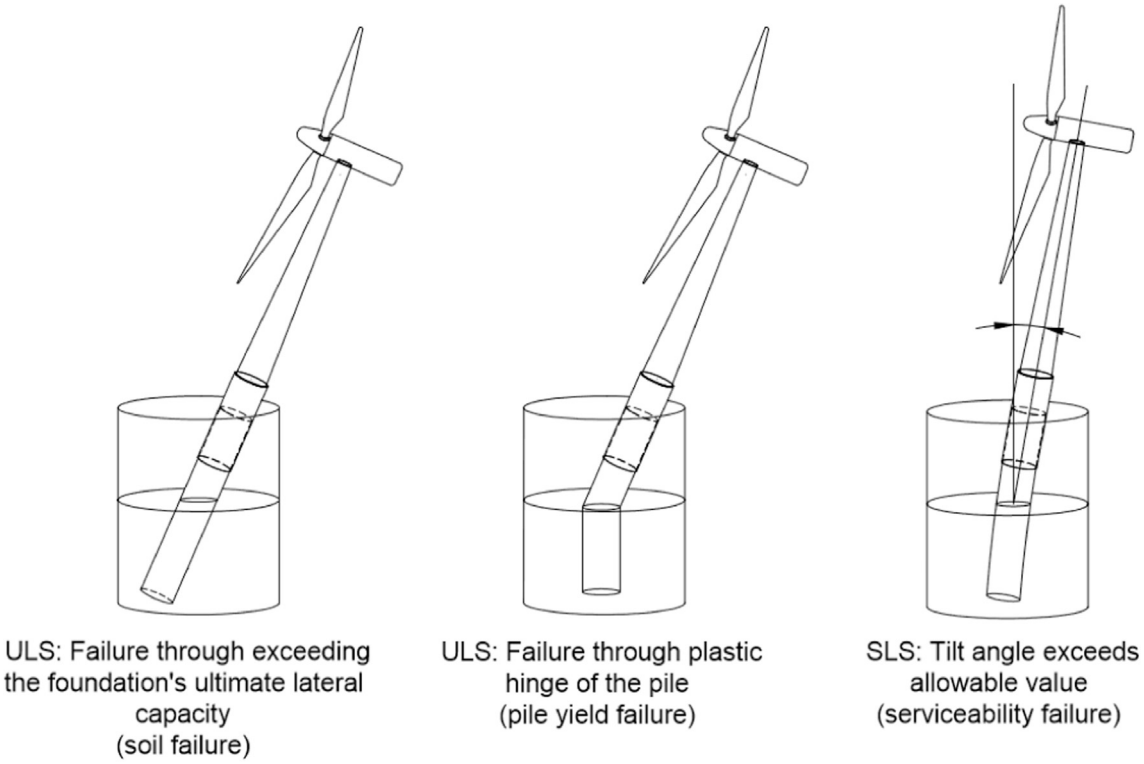

Fig. 1. Examples of ULS and SLS failure.

pile yield (structural) criteria.

(3) Use the initial pile dimensions to calculate wave loads and update foundation dimensions (if necessary).
(4) Check local and global stability (Euler/bar buckling and shell buckling) which will provide a minimum pile wall thickness. Thickness required related to pile driving stress should also be checked.
(5) Estimate the geotechnical load carrying capacity (vertical and lateral) of the foundation (i.e. check if soil fails first or the pile yields before the soil fails).
(6) Calculate foundation stiffness parameters (lateral, rocking and cross coupling stiffness) and estimate the mudline deformations and update foundation dimensions (if necessary).
(7) Calculate structural natural frequency of the whole system and carry out stability check. Apply dynamic amplification factors (DAFs) to compute the dynamic loads. Update foundation dimensions if necessary.
(8) Check natural frequency change over the lifetime of the structure.
(9) Check accumulated mudline deformations (deflection and rotation).
(10) Estimate fatigue life of foundation.

2. Calculation methodology

This section goes through the necessary calculations required to carry out the analysis detailed in the flowchart in Fig. 2 and the 10-step design described in the earlier section.

2.1. Optimizing initial pile dimensions (length, diameter and wall thickness)

In this section the methodology by which the pile dimensions can be selected is described. The key design drivers in choosing pile dimensions are based on Ultimate Limit State (ULS) and Serviceability Limit State (SLS) considerations. In this context, it may be mentioned that the monopile stiffness (which is a function of its bending stiffness of the monopile, soil stiffness and ground profile) dictates the structural natural frequency of the whole system including soil-structure interaction, and the compliance of the foundation for the prediction of pile head deflection and rotation. The pile geometry is defined with three key variables: pile diameter D_P, pile wall thickness t_P and embedded pile length L_P. Fig. 3 shows the influence of increasing these three parameters i.e. D_P, t_P and L_P on the bending stiffness of the monopile, structural natural frequency of the whole system, the pile head deflection and rotation calculated at the mudline. The results are plotted on dimensionless axes, given as changes from a baseline design in cohesionless soil.

From the figures one can draw several conclusions. The bending stiffness of the pile and the stiffness of the monopile foundation both scale with higher powers of the pile diameter. The bending stiffness increases only linearly with pile wall thickness. The embedded pile length, above a certain length (critical length), has limited effect on the foundation stiffness and thus on the structural natural frequency which are in line with the understanding of pile behaviour.

Based on above, the suggested method of choosing the initial pile dimensions and updating in subsequent design steps are as follows:

(1) The pile diameter is chosen (or increased) first, using it as an independent variable.
(2) The pile wall thickness may be expressed as a function of the pile diameter.
(3) The embedded length of the pile may be chosen based on a critical length which can be calculated based on pile diameter and relative pile soil stiffness ratio.

2.1.1. Diameter (D_P)

The pile diameter is chosen as an independent parameter, based on which the other dimensions are expressed. Initial pile diameter is chosen such that pile yield is avoided when the maximum wind load is acting on the structure. When updating foundation dimensions, the diameter is the key parameter for pile yield, soil resistance and structural natural frequency considerations. However, the mass of

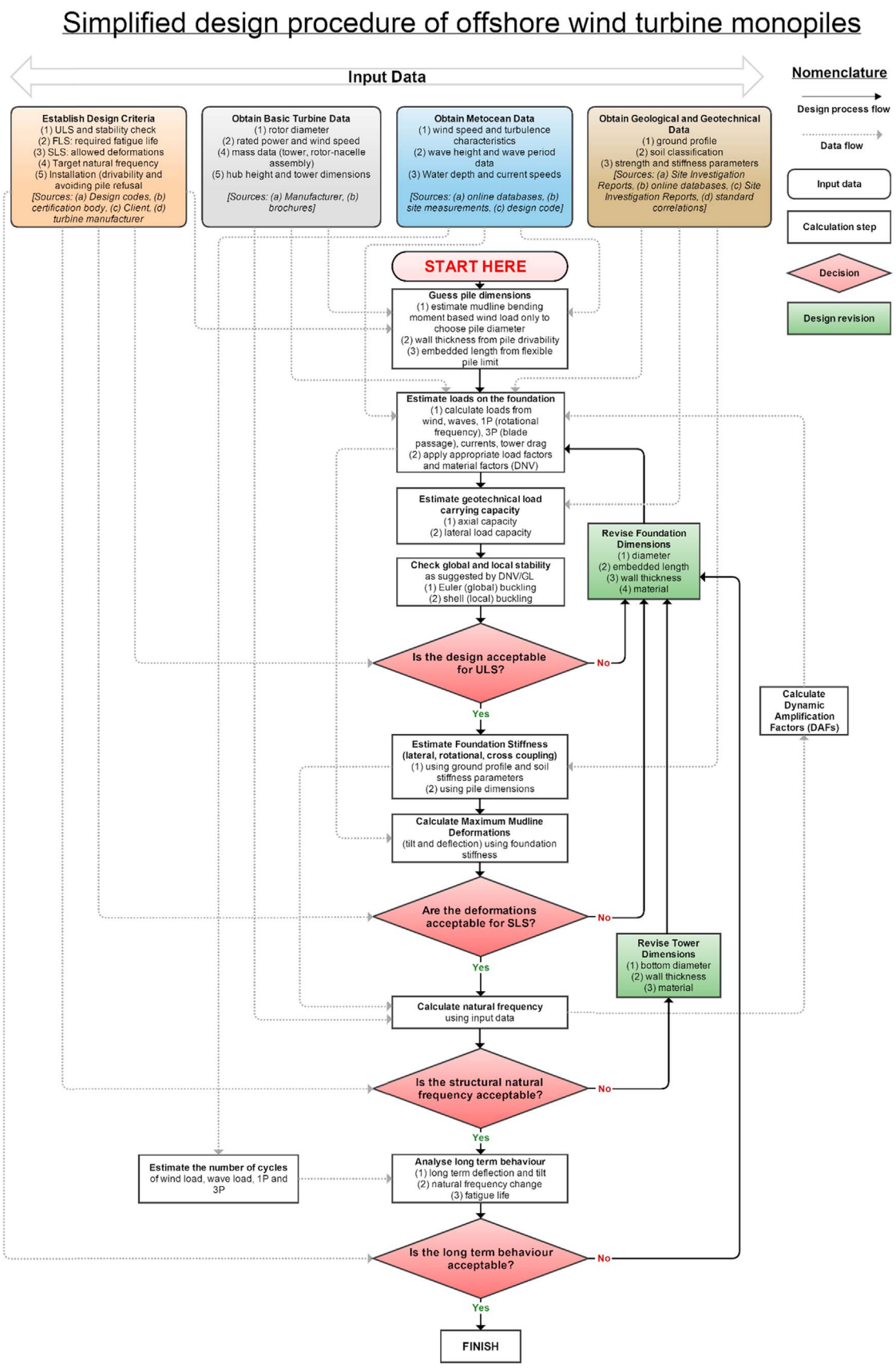

Fig. 2. Flowchart of the design process.

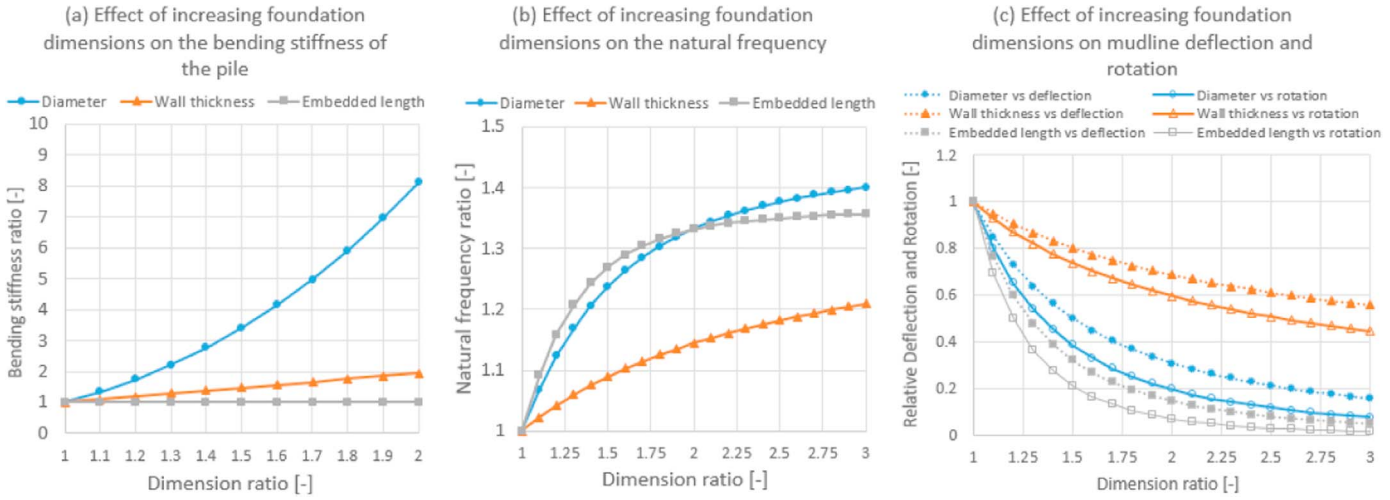

Fig. 3. Schematic figures of the effect of changing dimensions on (a) pile bending stiffness, (b) structural natural frequency, and (c) mudline deformations. Increases are measured from a typical baseline design.

the pile also increases with the second power of the diameter.

2.1.2. *Wall thickness* (t_P)

The initial value of wall thickness may be chosen according to API [7] as.

$$t_P \geq 6.35 + \frac{D_P}{100}\left[\text{mm}\right] \tag{1}$$

This wall thickness value may not necessarily provide sufficient stability to avoid local or global buckling of the pile, or to ensure that the pile can be driven into the seabed with the simplest installation method avoiding pile tip damage leading to early refusal. Therefore, these issues need to be addressed separately, as well as fatigue design of the pile, which may require additional wall thickness. Fig. 4 shows the wall thickness for installed offshore wind turbines of different monopile diameters. As can be seen, some piles have wall thicknesses significantly higher than the API required thickness. For details on buckling related issues (global buckling, avoiding local pile buckling or propagating pile tip damage due to installation), see Bhattacharya et al. [18], Aldridge et al. [2]. For practical reasons, the wall thickness is typically chosen based on standard plate thickness values to optimize manufacturing.

2.1.3. *Embedded length* (L_P)

The embedded length of a pile in the proposed simplified approach can be determined as a function of monopile diameter and relative pile-soil stiffness ratio. Several design criteria have been proposed for the necessary embedded length, see for example Kuo et al. [51] quoting Germanischer Lloyd [40] and an earlier version of DNV-OS-J101 [34]:

(1) Zero toe-kick criterion: the pile length is chosen such that the displacement of the pile toe is zero or negative.
(2) Vertical tangent criterion: the pile length is chosen such that the deflection curve has a vertical tangent at the pile toe.
(3) Critical pile length criterion: the pile length is chosen such that a further increase in pile length has no (or very limited) effect on the displacements (deflection and rotation) at the pile head. In other words, loosely speaking the depth to which the lateral loads from the pile head are being transferred.

Kuo et al. [51] and Achmus et al. [4] consider approach (1) and (2) above impractical and unsuitable for monopile design. They also found that zero toe-kick criterion was overly conservative and that the vertical tangent criterion produced counter-intuitive embedded length requirements. Therefore, in this paper 3rd criteria is suggested.

The initial guess pile length can be obtained based on the available ground profile data. If the shear modulus data of the soil layers are known, Eqs. (2) and (3) are recommended. On the other hand, if modulus of subgrade reaction is available, Eqs. (4)–(7) can be used.

Based on the elastic continuum approach proposed by Randolph [69], the critical pile length can be expressed through the necessary ratio of pile length L_P to pile diameter D_P in terms of the modified shear modulus G^* of the soil and the equivalent Young's modulus of the pile (E_{eq}). With this the pile length is calculated from the diameter as

$$L_P \geq D_P \left(\frac{E_{eq}}{G^*}\right)^{\frac{2}{7}} \tag{2}$$

where $E_{eq}=E_P I_P/\left(\frac{D_P^4\pi}{64}\right)$, $G^*=G_S(1+\frac{3}{4}\nu_S)$ with G_S being the shear

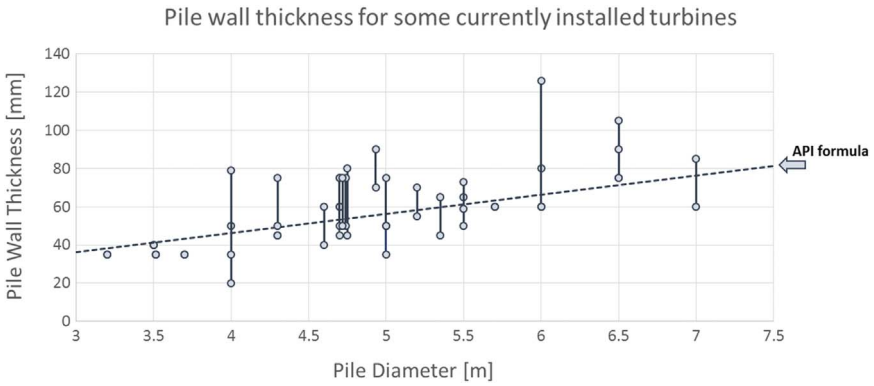

Fig. 4. Wall thickness of several currently installed wind turbines. The case studies used for the plot are collated in Appendix 1.

modulus of the soil averaged between the mudline and the pile embedment length, $E_P I_P$ is the pile's bending stiffness.

Carter and Kulhawy [28] present an expression to determine whether the pile can be considered rigid using a similar approach to that of Randolph [69] whereby the pile is rigid if

$$L_P \leq 0.05 D_P \left(\frac{E_{eq}}{G^*}\right)^{\frac{1}{2}} \tag{3}$$

Another approach is shown in Poulos and Davis [66] following Barber [14] using the soil's modulus of subgrade reaction k_h. In cohesive soils (which applies to Over-consolidated clayey ground profile), the modulus of subgrade reaction k_h can be considered constant with depth. The pile can be considered slender (infinitely long) if

$$L_P > 2.5 \left(\frac{E_P I_P}{k_h D_P}\right)^{\frac{1}{4}} \tag{4}$$

and the pile can be considered rigid if

$$L_P < 1.5 \left(\frac{E_P I_P}{k_h D_P}\right)^{\frac{1}{4}} \tag{5}$$

In normally consolidated clay or cohesionless soils (sand), the modulus of subgrade reaction approximately increases linearly with depth according to $k_h = n_h(z/D_P)$. In such soils he pile can be considered slender if

$$L_P > 4.0 \left(\frac{E_P I_P}{n_h}\right)^{\frac{1}{5}} \tag{6}$$

and the pile can be considered rigid if

$$L_P < 2.0 \left(\frac{E_P I_P}{n_h}\right)^{\frac{1}{5}} \tag{7}$$

These formulae can be used to obtain the necessary length as a function of pile diameter and soil stiffness.

2.1.4. Platform height above mudline (L_S)

The platform height is typically defined as the height of the top of the transition piece (which is also the bottom of the tower) above the Lowest Astronomical Tide (LAT) level. Here, however, we define the platform height (L_S) as the distance between the top of the transition piece (i.e. bottom of the tower) and the mudline.

The platform height above mudline is determined following DNV [34]. The High Water Level (HWL) with 50 year return period, considering astronomical tide above Mean Water Level (MWL) and positive storm surge, may be taken as the basis. The 50-year highest expected wave crest (here taken as $\eta_{50} = H_m$) and an air gap has to be added which is chosen here as $g_A = 0.2 H_{S,50}$, where $H_{S,50}$ is the significant wave height with a return period of 50 years. The platform height above mudline is then expressed as

$$L_S = HWL + \eta_{50} + g_A = S + H_{m,50} + 0.2 H_{S,50} \tag{8}$$

From the point of view of pile design, the platform height is important for the global structural natural frequency of the whole system and the total required length of the monopile (including the embedded length and the section above mudline). The natural frequency of the whole structure strongly depends on the flexibility of the substructure expressed by the substructure flexibility coefficient C_S in the formulation which is described in Section 2.6. Therefore, evaluating the necessary platform level above mudline L_S is important from the point of view of required monopile dimensions. The platform height also influences the total weight of the structure and therefore the total vertical load V on the foundation.

2.1.5. Substructure diameter

The tower is typically connected to the monopile via a transition piece. A gap of t_G is kept between the monopile and the transition piece for the grout, and a transition piece of wall thickness t_{TP} is used. When calculating the wave loads on the substructure, it is important to use the total diameter of the substructure D_S, which is equivalent to the transition piece diameter D_{TP} and is typically higher than the monopile diameter. D_S is given as

$$D_S = D_{TP} = D_P + 2t_G + 2t_{TP} \tag{9}$$

The diameter and wall thickness of the transition piece will also influence the deadweight of the structure and thus total vertical load V on the foundation, as well as the natural frequency.

2.2. Obtaining loads on the foundation (overturning moment, Shear load and vertical load)

The loads acting on the wind turbine rotor and substructure are ultimately transferred to the foundation and can be classified into two types: static or dead load due to the self-weight of the components and the cyclic/dynamic loads arising from the wind, wave, 1P and 3P loads, for further details see Arany et al. [9]. However, the challenging part is the dynamic loads acting on the wind turbine and the salient points are discussed below:

(a) The rotating blades apply a cyclic/dynamic lateral load at the hub level (top of the tower) and this load is determined by the turbulence intensity in the wind speed. The magnitude of dynamic load component depends on the turbulent wind speed component;
(b) The waves crashing against the substructure apply a lateral load close to the foundation. The magnitude of this load depends on the wave height and wave period, as well as the water depth;
(c) The mass imbalance of the rotor and hub and the aerodynamic imbalances of the blades generate vibration at the hub level and apply lateral load and overturning moment. This load has a frequency equal to the rotational frequency of the rotor (referred to as 1P loading in the literature). Since most of the industrial wind turbines are variable speed machines, 1P is not a single frequency but a frequency band between the frequencies associated with the lowest and the highest rpm (revolutions per minute);
(d) The blade shadowing effects (referred to as 2P/3P in the literature) also apply loads on the tower. This is a dynamic load having frequency equal to three times the rotational frequency of the turbine (3P) for three bladed wind turbines and two times (2P) the rotational frequency of the turbine for two bladed turbines. Rotational sampling of the turbulence by the blades and wind shear may also produce 2P/3P loads at the foundation. The 2P/3P excitations also act in a frequency band like 1P and is simply obtained by multiplying the limits of the 1P band by the number of the turbine blades.

A calculation procedure is developed in Arany et al. [9] which can be easily carried out in a spreadsheet program. The output of such a calculation will be relative wind and the wave loads and an example is shown in Fig. 5 where it is assumed that the wind and wave are perfectly aligned. This is a fair assumption for deeper water in projects further offshore where the fetch distance is high.

The peak frequency of the wind turbulence can be obtained theoretically from the Kaimal spectrum (suggested in the DNV code [34]). In the absence of site specific data, and for foundation design purposes, the wind load can be assumed to act at the hub level with a time period for wind given by $T = 4L_k/\overline{U}$ (where L_k is the integral length scale and $\overline{U}$ is the wind speed). Typical values are about 100 s as shown in Fig. 5.

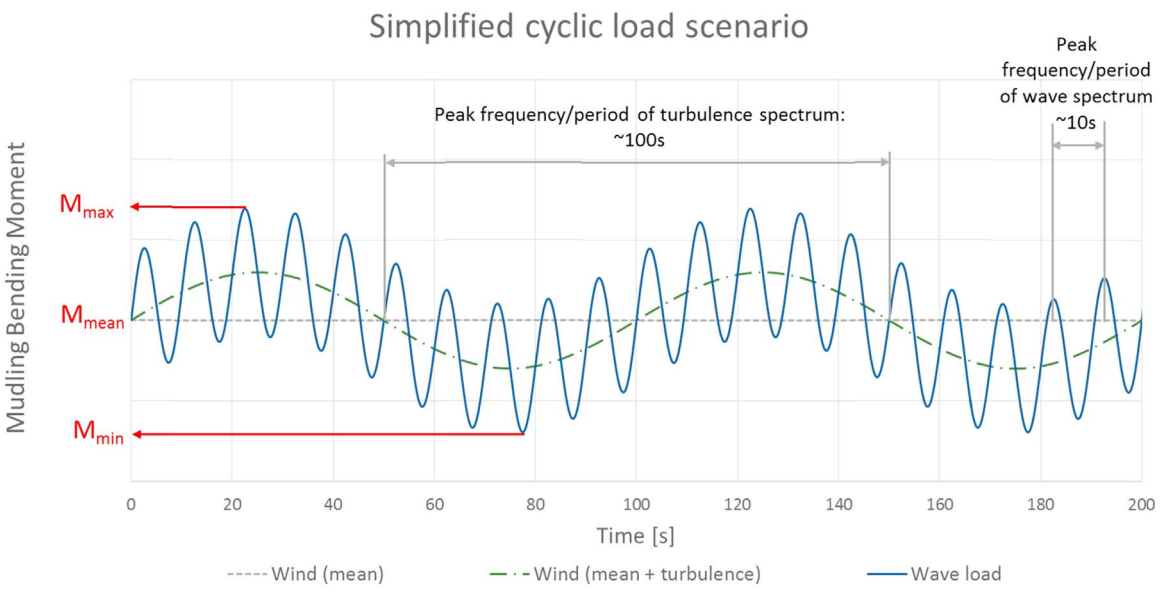

Fig. 5. Mudline moment due to wind and wave load, wind and waves collinear.

2.2.1. Load cases for foundation design

IEC codes [44–46] as well as the DNV code [34] describe hundreds of load cases that need to be analysed to ensure the safe operation of wind turbines throughout their lifetime of 20–30 years. However, in terms of foundation design, not all these cases are significant or relevant. The main design requirements for foundation design as explained in Section 1 are ULS, FLS and SLS. Five load cases important for foundation design are identified and described in Table 1.

All design load cases are built as a combination of four wind and four sea states. The wind conditions are:

(1) Normal turbulence scenario: the mean wind speed is the rated wind speed (U_R) where the highest thrust force is expected, and the wind turbulence is modelled by the Normal Turbulence Model (NTM). The NTM standard deviation of wind speed is defined in IEC [44].
(2) Extreme turbulence scenario: the mean wind speed is the rated wind speed (U_R), and the wind turbulence is very high, the Extreme Turbulence Model (ETM) is used. The ETM standard deviation of wind speed is defined in IEC [44].
(3) Extreme gust at rated wind speed scenario: the mean wind speed is the rated wind speed (U_R) and the 50-year Extreme Operating Gust (EOG) calculated at U_R hits the rotor. The EOG is a sudden change in the wind speed and is assumed to be so fast that the pitch control of the wind turbine has no time to alleviate the loading. This assumption is very conservative and is suggested to be used for simplified foundation design. The EOG speed is defined in IEC [44].
(4) Extreme gust at cut-out scenario: the mean wind speed is slightly below the cut-out wind speed of the turbine (U_{out}) and the 50-year Extreme Operating Gust (EOG) hits the rotor. Due to the sudden change in wind speed the turbine cannot shut down. Note that the EOG speed calculated at the cut-out wind speed is different from that evaluated at the rated wind speed [44].

The wave conditions are:

(1) 1-year Extreme Sea State (ESS): a wave with height equal to the 1-year significant wave height $H_{S,1}$ acts on the substructure.
(2) 1-year Extreme Wave Height (EWH): a wave with height equal to the 1-year maximum wave height $H_{m,1}$ acts on the substructure.
(3) 50-year Extreme Sea State (ESS): a wave with height equal to the 50-year significant wave height $H_{S,50}$ acts on the substructure.
(4) 50-year Extreme Wave Height (EWH): a wave with height equal to the 50-year maximum wave height $H_{m,50}$ acts on the substructure.

The 1-year ESS and EWH are used as a conservative overestimation of the Normal Wave Height (NWH) prescribed in IEC [45]. It is important to note here in relation to the Extreme Sea State (ESS) that the significant wave height and the maximum wave height have different meanings. The significant wave height H_S is the average of the highest one third of all waves in the 3-h sea state, while the maximum wave height H_m is the single highest wave in the same 3-h sea state.

Table 1
Representative design environmental scenarios as load cases chosen for foundation design.

#	Name & description	Wind model	Wave model	Alignment
E-1	Normal operational conditions *Wind and wave act in the same direction (no misalignment).*	NTM at U_R (U-1)	1-year ESS (W-1)	Collinear
E-2	Extreme wave load scenario *Wind and wave act in the same direction (no misalignment).*	ETM at U_R (U-2)	50-year EWH (W-4)	Collinear
E-3	Extreme wind load scenario *Wind and wave act in the same direction (no misalignment).*	EOG at U_R (U-3)	1-year EWH (W-2)	Collinear
E-4	Cut-out wind speed and Extreme Operating Gust scenario *Wind and wave act in the same direction (no misalignment).*	EOG at U_{out} (U-4)	50-year EWH (W-4)	Collinear
E-5	Wind-wave misalignment scenario *Same as E-2, except the wind and wave are misaligned at an angle of $\phi = 90°$. The dynamic amplification is higher in the cross-wind direction due to low aerodynamic damping.*	ETM at U_R (U-2)	50-year EWH (W-4)	Misaligned at $\phi = 90°$

According to the relevant standards [34,44,45], in the probability envelope of environmental states the most severe states with a 50-year return period has to be considered, and not 50-year return conditions for wind and wave unconditionally (separately). Indeed, extreme waves and high wind speeds tend to occur at the same time, however, the highest load due to wind is not expected when the highest wind speeds occur. This is partly because the pitch control alleviates the loading above the rated wind speed, but also because turbines shut down at high wind speeds for safety reasons. Idle or shut-down turbines, as well as turbines operating close to the cut-out wind speed have a significantly reduced thrust force acting on them compared to the thrust force at the rated wind speed due to the reduced thrust coefficient, as shown in Figs. 6 and 7.

The highest wind load is expected to be caused by scenario (U-3) and the highest wave load is due to scenario (W-4). In practice, the 50-year extreme wind load and the 50-year extreme wave load have a negligible probability to occur at the same time, and the DNV code also doesn't require these extreme load cases to be evaluated together [34]. The designer has to find the most severe event with a 50-year return period based on the joint probability of wind and wave loading.

Therefore, in this study, for the ULS analysis, two combinations are suggested:

(1) the Extreme Turbulence Model (ETM) wind load at rated wind speed combined with the 50-year Extreme Wave Height (EWH) – the combination of wind scenario (U-2) and wave scenario (W-4). This will provide higher loads in deeper water with higher waves.
(2) the 50-year Extreme Operating Gust (EOG) wind load combined with the 1-year maximum wave height. This will provide higher loads in shallow water in sheltered locations where wind load dominates

These scenarios are somewhat more conservative than those required by standards, which is to account for the simplified analysis approach chosen for this methodology. From the point of view of SLS and FLS, the single largest loading on the foundation is not representative, because the structure is expected to experience this level of loading only once throughout the lifetime. Following S-N curves for FLS and existing models for accumulated tilt and deflection of monopile foundations for SLS, it should also be noted that vibrations

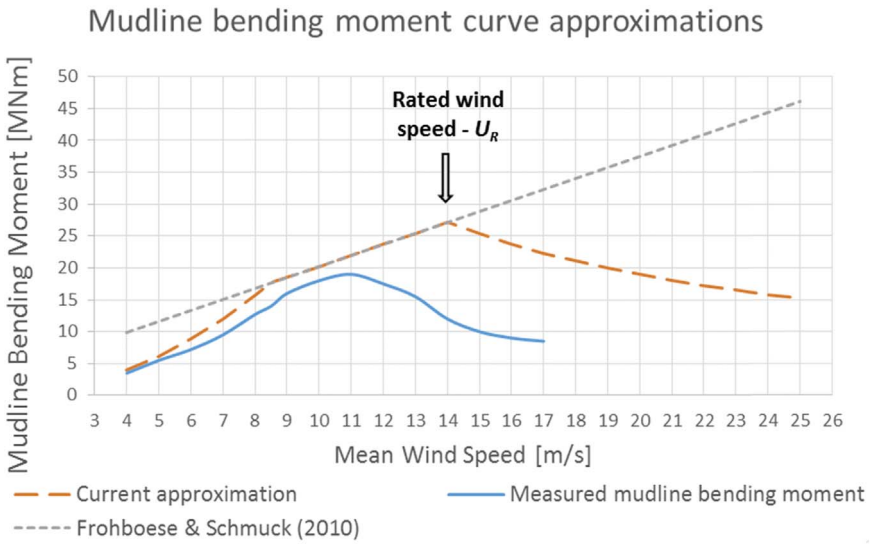

Fig. 6. Measured and approximated mudline bending moments of Horns Rev offshore wind turbine. The measured data is obtained from Hald et al. [41].

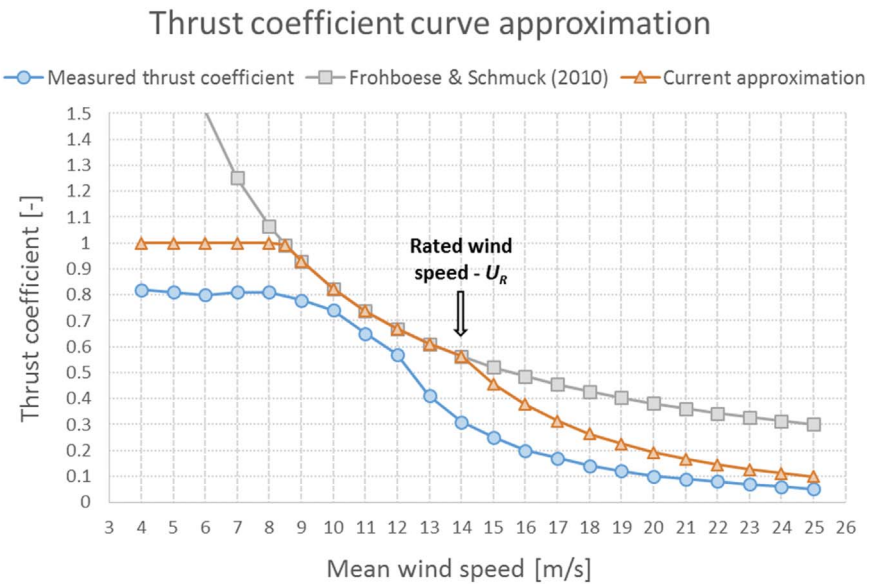

Fig. 7. Measured [41] and approximate thrust coefficients of the Vestas V80 turbine at Horns Rev.

with low magnitudes cause negligible damage and accumulated rotation/deflection.

The load cases in Table 1 are considered to be representative of typical foundation loads in a conservative manner and may serve as the basis for conceptual design of foundations. However, detailed analysis for design optimisation and the final design may require addressing other load cases as well. These analyses require detailed data about the site (wind, wave, current, geological, geotechnical, bathymetry data, etc) and also the turbine (blade profiles, twist and chord distributions, lift and drag coefficient distributions, control parameters and algorithms, drive train characteristics, generator characteristics, tower geometry, etc).

2.2.2. Wind load

The thrust force (Th) on a wind turbine rotor due to wind can be estimated in a simplified manner as

$$Th=\frac{1}{2}\rho_a A_R C_T U^2 \tag{10}$$

where ρ_a is the density of air, A_R is the rotor swept area, C_T is the thrust coefficient and U is the wind speed. The wind speed can range from cut-in to cut-out, with the appropriate thrust coefficient. The thrust coefficient can be approximated in the operational range of the turbine using three different sections (as shown in Figs. 6 and 7):

(1) Between cut-in (U_{in}) and rated wind speed (U_R) the method of Frohboese and Schmuck [38] may be followed

$$C_T=\frac{3.5[\frac{m}{s}](2U_R+3.5[\frac{m}{s}])}{U_R^2}\approx\frac{7[\frac{m}{s}]}{U_R} \tag{11}$$

(2) After rated wind speed, when the pitch control is active, the power is assumed to be kept constant, and thus the thrust coefficient is expressed as

$$C_T=3.5\left[\frac{m}{s}\right]U_R\left(2U_R+3.5\left[\frac{m}{s}\right]\right)\cdot\frac{1}{U^3}\approx 7\left[\frac{m}{s}\right]\cdot\frac{U_R^2}{U^3} \tag{12}$$

(3) The thrust coefficient is assumed not to exceed 1, therefore in the low wind speed regime where the formula of Frohboese and Schmuck [38] overestimates the thrust coefficient, the value is capped at 1.

When the wind speed is changing slowly, the thrust force follows the mean thrust curve as the pitch control follows the change in wind speed. However, when a sudden gust hits the rotor, the pitch control's time constant might be too high to follow the sudden change. If this is the case, then the thrust coefficient is 'locked' at its previous value while the wind speed in Eq. (11) changes to the increased wind speed due to the gust.

Assuming a quasi-static load calculation method, the wind speed can be divided into two parts, a mean wind speed $\overline{U}$ and a turbulent wind speed u component. For each load case, the mean wind speed $\overline{U}$ and the turbulent wind speed component u are defined separately, and the total wind speed is expressed as

$$U=\overline{U}+u \tag{13}$$

Using this assumption, the wind load can be separated into a mean thrust force (or static force) and a turbulent thrust force (or dynamic force).

$$Th=Th_{mean}+Th_{turb}=\frac{1}{2}\rho_a A_R C_T \overline{U}^2+\frac{1}{2}\rho_a A_R C_T (2\overline{U}u+u^2) \tag{14}$$

In this equation the thrust coefficient C_T is calculated as shown in Eq. (11).

Fig. 6 plots the measured mean mudline bending moment for a Vestas V80 wind turbine at the Horns Rev offshore wind farm obtained from Hald et al. [41] and compares it with the approximation based on Eqs. (10)–(14). This is based on the measured thrust force acting at the hub level and the corresponding thrust coefficient is shown in Fig. 7.

The maximum thrust force occurs around the rated wind speed (or more specifically, before the pitch control activates). In reality, the pitch control activates somewhat below the rated wind speed (as can be seen in Fig. 7). This is to ensure a smooth transition between the section where the power is proportional to the cube of the wind speed and the pitch controlled region where the power is kept constant, in order and avoid repeated switching around the rated wind speed [22]. Therefore, in the measured scenario the maximum of the thrust force (and thus the bending moment) occurs at around 11[m/s], as opposed to the theoretical approximation, in which the maximum is at U_R=14[m/s]. Taking the maximum to be at U_R is, however, conservative due to the formula used for the approximation. If the value of 11[m/s] is substituted into the formula in Eq. (10), one still arrives at a conservative approximation for the mean thrust force, and therefore this value (at which pitch control activates) may also be used. It should be noted, however, that typically the nature of the pitch control mechanism and the thrust coefficient curve of the turbine are not available in the early design phases. Consequently, the use of U_R is suggested, which is typically available and produces a conservative approximation.

2.2.3. Wind scenario (U-1): Normal Turbulence (NTM) at rated wind speed (U_R)

This scenario is typical for normal operation of the turbine. The standard deviation of wind speed in normal turbulence following IEC [44] can be written as

$$\sigma_{U,NTM}=I_{ref}(0.75U+b) \text{ with } b=5.6[m/s] \tag{15}$$

where I_{ref} is the reference turbulence intensity (expected value at U = 15[m/s]).

For the calculation of the maximum turbulent wind speed component u_{NTM}, the time constant of the pitch control is assumed to be the same as the time period of the rotation of the rotor. In other words, it is assumed that the pitch control can follow changes in the wind speed that occur at a lower frequency than the rotational speed of the turbine ($f_{1P,max}$=0.217[Hz]). Then u_{NTM} may be determined by calculating the contribution of variations in the wind speed with a higher frequency than $f_{1P,max}$ to the total standard deviation of wind speed. From the Kaimal spectrum used for the wind turbulence process, this can be calculated using Eq. (16).

$$\sigma_{U,NTM,f>f_{1P}}=\sqrt{\int_{f_{1P,max}}^{\infty}S_{uu}(f)df}=\sigma_{U,NTM}\sqrt{\int_{f_{1P,max}}^{\infty}\frac{\frac{4L_k}{U_R}}{\left(1+\frac{6L_k}{U_R}f\right)^{\frac{5}{3}}}df}=\sigma_{U,NTM}\sqrt{\frac{1}{\left(\frac{6L_k}{U_R}f_{1P,max}+1\right)^{\frac{2}{3}}}} \tag{16}$$

The turbulent wind speed encountered in normal operation in normal turbulence conditions is found by assuming normal distribution of the turbulent wind speed component and taking the 90% confidence level value. This is substituted into the quasi-static equation used in Eq. (14).

$$u_{NTM}=1.28\sigma_{U,NTM,f>f_{1P}} \tag{17}$$

$$F_{wind,NTM}=\frac{1}{2}\rho_a A_R C_T (U_R+u_{NTM})^2 \tag{18}$$

$$M_{wind,NTM}=F_{wind,NTM}(S+z_{hub}) \tag{19}$$

2.2.4. Wind scenario (U-2): Extreme Turbulence (ETM) at rated wind speed (U_R)

The Extreme Turbulence Model (ETM) is used to calculate the standard deviation of wind speed at the rated wind speed, and from that the maximum wind load under normal operation in extreme turbulence conditions. The standard deviation of wind speed in ETM is given in IEC [44] as

$$\sigma_{U,ETM}=cI_{ref}\left[0.072\left(\frac{U_{avg}}{c}+3\right)\left(\frac{U_R}{c}-4\right)+10\right] \text{ with } c=2\,[\mathrm{m/s}] \tag{20}$$

where U_{avg} is the long term average wind speed at the site. The maximum turbulent wind speed component u_{ETM} is determined similarly to the previous case.

$$\sigma_{U,ETM,f>f_{1P}}=\sqrt{\int_{f_{1P,max}}^{\infty}S_{uu}(f)df}=\sigma_{U,ETM}\sqrt{\int_{f_{1P,max}}^{\infty}\frac{\frac{4L_k}{U_R}}{\left(1+\frac{6L_k}{U_R}f\right)^{\frac{5}{3}}}df}$$
$$=\sigma_{U,ETM}\sqrt{\frac{1}{\left(\frac{6L_k}{U_R}f_{1P,max}+1\right)^{\frac{2}{3}}}} \tag{21}$$

The turbulent wind speed encountered in normal operation in extreme turbulence conditions, which is used for cyclic/dynamic load analysis, is found by assuming normal distribution of the turbulent wind speed component. As opposed to the normal turbulence situations, the 95% confidence level value is taken. This is substituted into the quasi-static equation used in Eq. 14.

$$u_{ETM}=2\sigma_{U,ETM,f>f_{1P}} \tag{22}$$

$$F_{wind,ETM}=\frac{1}{2}\rho_a A_R C_T(U_R+u_{ETM})^2 \tag{23}$$

$$M_{wind,ETM}=F_{wind,ETM}(S+z_{hub}) \tag{24}$$

2.2.5. Wind scenario (U-3): Extreme Operating Gust (EOG) at rated wind speed (U_R)

The maximum force is assumed to occur when the maximum mean thrust force acts and the 50-year Extreme Operating Gust (EOG) hits the rotor. Due to this sudden gust, the wind speed is assumed to change so fast that the pitch control doesn't have time to adjust the blade pitch angles. This assumption is very conservative as the pitch control in reality has a time constant which would allow for some adjustment of the blade pitch.

The methodology for the calculation of the magnitude of the 50 year extreme gust is described in DNV [34]. This methodology builds on the long term distribution of 10-min mean wind speeds at the site, which is typically represented by a Weibull distribution. The Cumulative Distribution Function (CDF) can be written in the following form

$$\Phi_{U10}(K,\ s)=1-e^{-\left(\frac{U}{K}\right)^s} \tag{25}$$

where K and s are the Weibull scale and shape parameters, respectively. From this the CDF of 1-year wind speeds can be obtained using

$$\Phi_{U10,1-year}(K,\ s)=\Phi_{U10}(K,\ s)^{52596} \tag{26}$$

where the number 52,596 represents the number of 10-min intervals in a year($52596=365.25[days/year]\cdot 24[h/day]\cdot 6[10min\ intervals/h]$).

From this the 50-year extreme wind speed, which is typically used in wind turbine design for extreme wind conditions, can be determined by the wind speed at which the CDF is 0.98 (that is, 1-year 10-min mean wind speed that has 2% probability).

$$U_{10,50-year}=K\left[-ln\left(1-0.98^{\frac{1}{52596}}\right)\right]^{\frac{1}{s}} \tag{27}$$

The extreme gust speed is then calculated at the rated wind speed from

$$u_{EOG}=min\left\{1.35(U_{10,1-year}-U_R);\ \frac{3.3\sigma_{U,c}}{1+\frac{0.1D}{\Lambda_1}}\right\} \tag{28}$$

where D is the rotor diameter, $\Lambda_1=L_k/8$ with L_k being the integral length scale, $\sigma_{U,c}=0.11U_{10,1-year}$ is the characteristic standard deviation of wind speed, $U_{10,1-year}=0.8U_{10,50-year}$. Using this, the total wind load is estimated as

$$F_{wind,EOG}=Th_{EOG}=\frac{1}{2}\rho_a A_R C_T(U_R+u_{EOG})^2 \tag{29}$$

and using the water depth S and the hub height above sea level z_{hub}, the mudline bending moment (without the load factor γ_L) is given as

$$M_{wind,EOG}=F_{wind,EOG}(S+z_{hub}) \tag{30}$$

2.2.6. Wind scenario (U-4): Extreme Operating Gust (EOG) at the cut-out wind speed (U_{out})

This load case is examined here because intuitively it may seem natural to expect the highest loads when the turbine is operating at the highest operational wind speed, however, this is not the case. Wind load caused by the Extreme Operating Gust (EOG) at the highest operational wind speed (the cut-out wind speed U_{out}) is calculated taking into consideration that the thrust coefficient expression of Frohboese and Schmuck [38] is no longer valid. The thrust coefficient is determined from the assumption that the pitch control keeps the power constant. This means that the thrust force is inversely proportional to the wind speed above rated wind speed U_R and the thrust coefficient is inversely proportional to the cube of the wind speed.

$$C_T=\frac{7[\frac{m}{s}]U_R^2}{U^3} \tag{31}$$

The Extreme Operating Gust speed at cut-out wind speed $u_{EOG,U_{out}}$ is determined as given in (note that this differs for different mean wind speeds, i.e. the value is not the same at U_R and at U_{out}). The thrust force and moment are then given by:

$$T_{wind,U_{out}}=\frac{1}{2}\rho_a A_R C_T(U_{out})(U_{out}+u_{EOG,U_{out}})^2 \tag{32}$$

$$M_{wind,U_{out}}=(S+z_{hub})T_{wind,U_{out}} \tag{33}$$

2.2.7. Wave load

A simplified approach to wave load estimation is Morison's (or MOJS) equation [63]. In these equations the diameter of the substructure is taken as $D_S=D_P+2t_{TP}+2t_G\,[m]$ to account for the transition piece (TP) and the grout (t_G) thickness, as given in Section 2.1.5 in Eq. (9). The circular substructure area A_S is also calculated from this diameter. The methodology in this paper builds on linear (Airy) wave theory, which gives the surface elevation η, horizontal particle velocity w and the horizontal particle acceleration $\dot{w}$ as

$$\eta(x,\ t)=\frac{H_m}{2}\cos\left(\frac{2\pi t}{T_S}-kx\right) \tag{34}$$

$$w(x,\ z,\ t)=\frac{\pi H_m\cosh(k(S+z))}{T_S\sinh(kS)}\cos\left(\frac{2\pi t}{T_S}-kx\right) \tag{35}$$

$$\dot{w}(x,\ z,\ t)=\frac{-2\pi^2 H_m\cosh(k(S+z))}{T_S^2\sinh(kS)}\sin\left(\frac{2\pi t}{T_S}-kx\right) \tag{36}$$

where x is the horizontal coordinate in the along-wind direction ($x = 0$ at the turbine, see Fig. 8) and the wave number k is obtained from the dispersion relation

$$\omega^2 = gk \tanh(kS) \text{ with } \omega = \frac{2\pi}{T_S} \tag{37}$$

.

The force on a unit length strip of the substructure is the sum of the drag force F_D and the inertia force F_I

$$dF_{wave}(z,\ t) = dF_D(z,\ t) + dF_I(z,\ t) = \frac{1}{2}\rho_w D_S C_D w(z,\ t)|w(z,\ t)| + C_m \rho_w A_S \dot{w}(z,\ t) \tag{38}$$

where C_D is the drag coefficient, C_m is the inertia coefficient, ρ_w is the density of seawater. The total horizontal force and bending moment at the mudline is then given by integration as

$$F_{wave}(t) = \int_{-S}^{\eta} dF_D dz + \int_{-S}^{\eta} dF_I dz \tag{39}$$

$$M_{wave}(t) = \int_{-S}^{\eta} dF_D (S + z_{hub}) dz + \int_{-S}^{\eta} dF_I (S + z_{hub}) dz \tag{40}$$

The peak load of the drag and inertia loads occur at different time instants, and therefore the maxima are evaluated separately. The maximum of the inertia load occurs at the time instant $t = 0$ when $\eta = 0$ and the maximum of the drag load occurs when $t = T_S/4$ and $\eta = H_m/2$. The maximum load is then obtained by carrying out the integrations:

$$F_{D,max} = \frac{1}{2}\rho_w D_S C_D \frac{\pi^2 H_S^2}{T_S^2 \sinh^2(kS)} P_D(k,\ S,\ \eta) \tag{41}$$

$$M_{D,max} = \frac{1}{2}\rho_w D_S C_D \frac{\pi^2 H_S^2}{T_S^2 \sinh(kS)} Q_D(k,\ S,\ \eta) \tag{42}$$

$$P_D(k,\ S,\ \eta) = \frac{e^{2k(S+\eta)} - e^{-2k(S+\eta)}}{8k} + \frac{S+\eta}{2} \tag{43}$$

$$Q_D(k,\ S,\ \eta) = \left(\frac{S+\eta}{8k} - \frac{1}{16k^2}\right) e^{2k(S+\eta)} - \left(\frac{S+\eta}{8k} + \frac{1}{16k^2}\right) e^{-2k(S+\eta)} + \left(\frac{S+\eta}{2}\right)^2 + \frac{1}{8k^2} \tag{44}$$

$$F_{I,max} = \frac{1}{2}\rho_w C_m D_S^2 \frac{\pi^3 H_S}{T_S^2 \sinh(kS)} P_I(k,\ S,\ \eta) \tag{45}$$

$$M_{I,max} = \frac{1}{2}\rho_w C_m D_S^2 \frac{\pi^3 H_S}{T_S^2 \sinh(kS)} Q_I(k,\ S,\ \eta) \tag{46}$$

$$P_I(k,\ S,\ \eta) = \frac{\sinh(k(S+\eta))}{k} \tag{47}$$

$$Q_I(k,\ S,\ \eta) = \left(\frac{S+n}{2k} - \frac{1}{2k^2}\right) e^{k(S+\eta)} - \left(\frac{S+\eta}{2k} - \frac{1}{2k^2}\right) e^{-k(S+\eta)} + \frac{1}{k^2} \tag{48}$$

In the simplified method for obtaining foundation loads, it can be conservatively assumed that the sum of the maxima of drag and inertia loads is the design wave load. This assumption is conservative, because the maxima of the drag load and inertia load occur at different time instants. All wave scenarios (W-1)-(W-4) are evaluated with the same procedure, using different values of wave height H and wave period T.

2.2.8. Vertical (deadweight) load

The total vertical load on the foundation is calculated as

$$V = mg \tag{49}$$

where m is the total mass of the structure

$$m = m_{RNA} + m_T + m_{TP} + m_P \tag{50}$$

where m_{RNA} is the total mass of the rotor-nacelle assembly, $m_T = \rho_T D_T \pi t_T L_T$ is the total weight of the tower, $m_{TP} = \rho_{TP}(D_P + 2t_G + t_{TP})\pi t_{TP} L_{TP}$ is the mass of the transition piece, $m_P = \rho_P D_P \pi t_P (L_P + L_S)$ is the mass of the pile.

2.3. Ultimate capacity of monopiles

In the simplified approach, the lateral and vertical capacity of piles

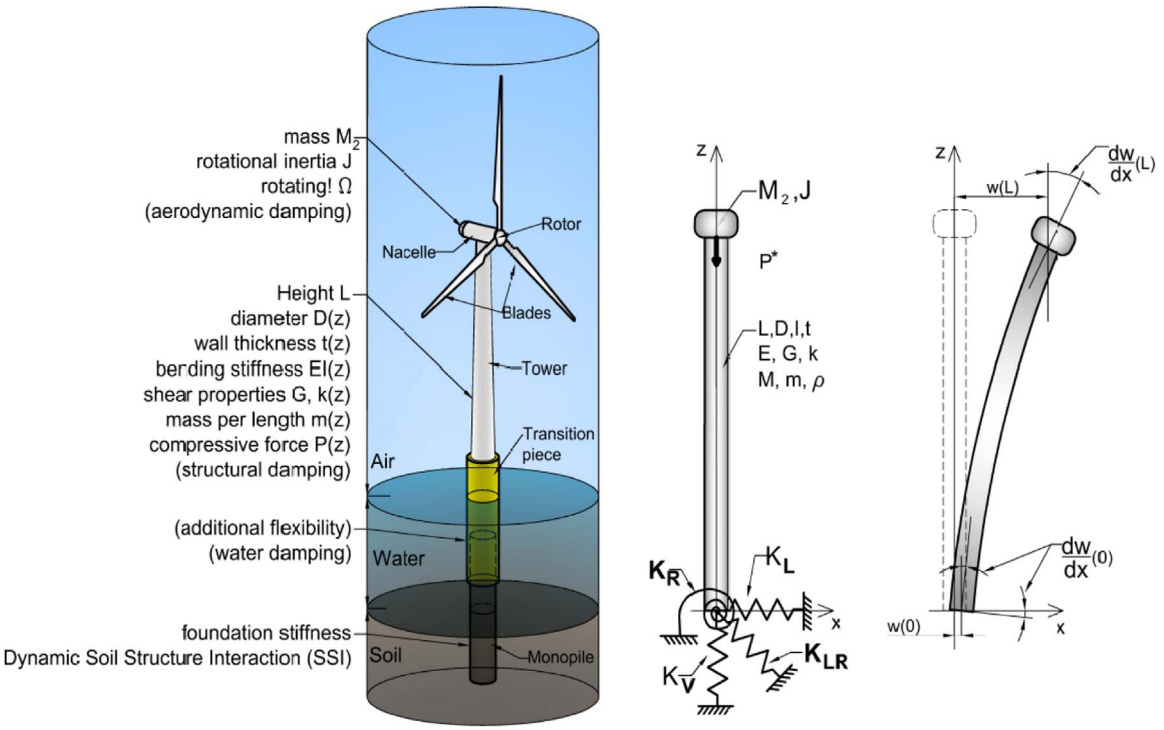

Fig. 8. Importance of foundation stiffness.

in cohesive and cohesionless soils can be calculated following Poulos and Davis [66] (for a more recent source see Randolph and Gourvenec [68]). Only the horizontal capacity is addressed here, because horizontal load and overturning moment are the driving constraints for typical monopiles, and if these requirements are addressed the vertical capacity is typically also satisfactory.

2.3.1. Constant soil resistance with depth

In ground conditions where the soil resistance is assumed to be constant with depth (OCR soils), and where soil fails first (i.e. the pile does not fail through a plastic hinge formation), the ultimate capacity can be calculated using the following formulae.

$$g=2(L_P+D_P+e) - \frac{\sqrt{16(L_P+D_P+e)^2-4(4L_Pe-2D_Pe+4D_PL_P-2.5D_P^2+2L_P^2)}}{2} \quad (51)$$

$$f=\frac{F_R}{9s_uD_P} \quad (52)$$

$$M_R=F_R(e+1.5D_P+0.5f)=2.25D_Pg^2s_u \quad (53)$$

$$L_P=1.5D_P+f+g \quad (54)$$

where s_u is the undrained shear strength, e is the eccentricity of loading (i.e. $/F$), M_R is the moment capacity of the pile, F_R is the horizontal load carrying capacity of the pile, D_P and L_P are the diameter and embedded length of the pile, respectively. For derivation and details please refer to Chapter 7 of Poulos and Davis [66].

2.3.2. Linear soil resistance with depth

In ground conditions, where the soil resistance is assumed to increase linearly with depth (e.g. some cohesionless soils and lightly overconsolidated clay), the horizontal load and moment capacity of a piled foundation, assuming that the soil fails first (no plastic hinge is formed in the pile), is expressed using the following equations:

$$F_R=\frac{0.5\gamma D_PL_P^3K_P}{e+L_P}=\frac{3}{2}\gamma' D_PK_Pf^2 \quad (55)$$

$$K_P=\frac{1+sin\phi'}{1-sin\phi'} \quad (56)$$

$$M_R=F_R\left(e+\frac{2}{3}f\right) \quad (57)$$

$$f=0.82\sqrt{\frac{F_R}{D_PK_P\gamma}} \quad (58)$$

where γ' is the submerged unit weight of the cohesionless soil (assumed constant with depth); D_P and L_P are the pile diameter and embedded length, respectively; e is the load eccentricity ($e = M/F$); ϕ' is the effective angle of internal friction; M_R and F_R are the moment and the horizontal load carrying capacity of the foundation, respectively. For derivation and details, refer to Chapter 7 of Poulos and Davis [66].

2.4. Foundation stiffness of monopiles

Traditionally in the offshore industry, a non-linear p-y method is employed to find out pile head deformations (deflection and rotation) and foundation stiffness. The approach can be found in API [7] and also suggested in DNV [34]. Originally it was developed by Matlock [59]; Reese etl. [70]; O'Neill and Murchinson [64] and the basis of this methodology is the Winkler approach [77] whereby the soil is modelled as independent springs along the length of the pile. The p-y approach uses non-linear springs and produces reliable results for the cases for which it was developed, i.e. small diameter piles and for few cycles of loading. The method is not validated for large diameter piles, in fact, using this method, under prediction of foundation stiffness has been reported by Kallehave and Thilsted [47], who also propose an updated p-y formulation. Many researchers have recently worked on developing design methodologies for the large diameter more stocky monopiles with length to diameter ratios typically in the range between 4 and 10. A new finite element analysis approach has been presented in Zdravkovic et al. [80], and a new design method has been proposed in Byrne et al. [24]. Field testing has also been carried out to improve understanding in Byrne et al. [26].

In this simplified framework a three springs approach (see Fig. 8) is suggested to take into account the foundation stiffness following Zaaijer [78]; Adhikari and Bhattacharya [5]; Adhikari and Bhattacharya [6]; Lombardi et al. [57]; Zania [79]; Damgaard et al. [31]; Arany et al. [8], Abed et al. [1]. Fig. 8 shows the definition of the foundation stiffness which is shown by K_V (vertical stiffness), K_L (Lateral stiffness) K_R (Rocking stiffness) and K_{LR} (Cross-Coupling). The input required to obtain K_L, K_R and K_R are: (a) pile dimensions; (b) ground profile (i.e. soil stiffness variation with depth (constant, linearly varying with depth or varying with square root of depth, see Fig. 9)); (c) soil stiffness at a depth of one pile diameter. Alternatively, some formulations define the soil with the modulus of subgrade reaction k_h or the coefficient of subgrade reaction n_h (the rate of increase of k_h with depth)..

The first step in the calculation procedure of the pile head stiffness is the classification of pile behaviour, i.e. whether the monopile will behave as a long flexible pile or a short rigid pile, and then using the appropriate relations to obtain K_L, K_R and K_{LR}. Please note that the vertical stiffness is not required for simplified calculations as the structure is very stiff vertically.

Rigid piles are short enough to undergo rigid body rotation in the soil under operational loads, instead of deflecting like a clamped beam. Slender piles on the other hand undergo deflection under operating loads and fail typically through the formation of a plastic hinge; the pile toe does not 'feel' the effects of the loading at the mudline and the pile can be considered 'infinitely long'. Formulae for determining whether a pile can be considered slender or rigid have been given in Section 2.1.3 in Eqs. 2–7.

As mentioned before, in the simplified procedure to obtain foundation stiffness two parameters are required to define the ground (soil stiffness at $1D_P$ below mudline denoted by E_{S0} and the stiffness profile i.e. variation with depth). The stiffness profile is expressed mathematically as

$$E_S(z)=E_{S0}\left(\frac{|z|}{D_P}\right)^n \quad (59)$$

where homogeneous, linear inhomogeneous and square root inhomogeneous profiles are given by $n = 0$, $n = 1$ and $n = 1/2$, respectively (see Fig. 9).

Analytical solutions are rarely available from a subgrade approach for general cases, but simplified expressions are available for rigid and slender piles [66]. Various approaches have been developed to correlate foundation loads (horizontal load F_x and bending moment M_y) to pile head deflection ρ and rotation θ. These expressions can be easily transformed into a matrix form of the load response in terms of three springs (K_L, K_{LR}, K_R). Some of the most common methods are found in Poulos and Davis [66] following Barber [14]) for both rigid and slender piles; Gazetas [39] also featured in Eurocode 8 Part 5 [37] developed for slender piles; Randolph [69] developed for slender piles in both homogeneous and linear inhomogeneous soils; Pender [65] developed for slender piles; Carter and Kulhawy [28] for rigid piles in rock; Higgins and Basu [43] for rigid piles; Shadlou and Bhattacharya [72] for both rigid and slender piles. The formulae for the foundation stiffness are summarized in Table 2 for slender piles and Table 3 for rigid piles.

Based on comparison of measured and predicted natural frequencies based on a three springs approach (see e.g. Arany et al. [12]), it is

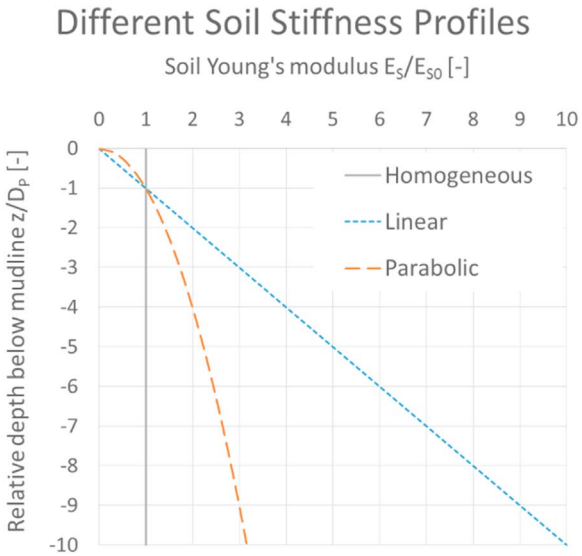

Fig. 9. Homogeneous, linear and parabolic soil stiffness profiles.

suggested that the best approach to estimate the foundation stiffness is the methods of Poulos and Davis [66] and Randolph [69]. Furthermore, in the authors' experience the slender pile formulae give stiffness results that produce better approximations of the Eigen frequency of the structure than the formulae for stocky (rigid) piles.

The foundation stiffness is required for two calculations: Deformation (deflection ρ and rotation θ at mudline) and natural frequency estimation. Few points may be noted regarding these springs:

(a) The properties and shape of the springs (load-deformation characteristics i.e. lateral load-deflection or moment-rotation) should be such that the deformation is acceptable under the working load scenarios expected in the lifetime of the turbine. Further details of shape of these springs associated with stress-strain of the supporting soil can be found in Bouzid et al. [19].
(b) The values of the springs (stiffness of the foundation) are necessary to compute the natural period of the structure using linear Eigen value analysis. Further details on the analysis required can be found in Adhikari and Bhattacharya [5]; Adhikari and Bhattacharya [6]; Arany et al. [8]; Arany et al. [12];
(c) The values of the springs will also dictate the overall dynamic stability of the system due to its non-linear nature. It must be mentioned that these springs are not only frequency dependent but also change with cycles of loading due to dynamic soil structure interaction. Further details on the dynamic interaction can be found in [16,17,31,57,79]

2.5. Deformation (SLS calculations)

The stiffness expressions in Tables 2 and 3 can be easily transformed into foundation compliance matrices (that is, from load/deformation units to deformation/load units). For brevity, the formulae here are omitted and the deformations are calculated directly from the stiffness values. A three springs model can be written with a stiffness matrix as the following:

$$\begin{bmatrix} F_x \\ M_y \end{bmatrix} = \begin{bmatrix} K_L & K_{LR} \\ K_{LR} & K_R \end{bmatrix} \begin{bmatrix} \rho \\ \theta \end{bmatrix} \tag{60}$$

where F_x is the lateral force in the direction of the x axis as defined in Fig. 8, M_y is the fore-aft overturning moment (around the y axis), K_L is the lateral spring, K_R is the rotational spring, K_{LR} is the cross coupling spring, ρ is the displacement in the x direction and $\theta = \partial\rho/\partial z$ is the slope of the deflection (tilt or rotation).

The deformations can then be easily expressed using

$$\rho = \frac{K_R}{K_L K_R - K_{LR}^2} F_x - \frac{K_{LR}}{K_L K_R - K_{LR}^2} M_y \tag{61}$$

$$\theta = -\frac{K_{LR}}{K_L K_R - K_{LR}^2} F_x + \frac{K_L}{K_L K_R - K_{LR}^2} M_y \tag{62}$$

Table 2
Stiffness formulae by different researchers for slender piles in various soil profiles.

Lateral stiffness K_L	Cross-coupling stiffness K_{LR}	Rotational stiffness K_R
Randolph [69], slender piles, both for homogeneous and linear inhomogeneous soils		
$\frac{1.67 E_{S0} D_P}{f_{(\nu S)}} \left(\frac{E_{eq}}{E_{S0}}\right)^{0.14}$	$-\frac{0.3475 E_{S0} D_P^2}{f_{(\nu S)}} \left(\frac{E_{eq}}{E_{S0}}\right)^{0.42}$	$\frac{0.1975 E_{S0} D_P^3}{f_{(\nu S)}} \left(\frac{E_{eq}}{E_{S0}}\right)^{0.7}$
Pender [65], slender piles, homogeneous soil		
$1.285 E_{S0} D_P \left(\frac{E_{eq}}{E_{S0}}\right)^{0.188}$	$-0.3075 E_{S0} D_P^2 \left(\frac{E_{eq}}{E_{S0}}\right)^{0.47}$	$0.18125 E_{S0} D_P^3 \left(\frac{E_{eq}}{E_{S0}}\right)^{0.738}$
Pender [65], slender piles, linear inhomogeneous soil		
$0.85 E_{S0} D_P \left(\frac{E_{eq}}{E_{S0}}\right)^{0.29}$	$-0.24 E_{S0} D_P^2 \left(\frac{E_{eq}}{E_{S0}}\right)^{0.53}$	$0.15 E_{S0} D_P^3 \left(\frac{E_{eq}}{E_{S0}}\right)^{0.77}$
Pender [65], slender piles, parabolic inhomogeneous soil		
$0.735 E_{S0} D_P \left(\frac{E_{eq}}{E_{S0}}\right)^{0.33}$	$-0.27 E_{S0} D_P^2 \left(\frac{E_{eq}}{E_{S0}}\right)^{0.55}$	$0.1725 E_{S0} D_P^3 \left(\frac{E_{eq}}{E_{S0}}\right)^{0.776}$
Poulos and Davis [66] following Barber [14], slender pile, homogeneous soil		
$\frac{k_h D_P}{\beta}$	$-\frac{k_h D_P}{\beta^2}$	$\frac{k_h D_P}{2\beta^3}$
Poulos and Davis [66] following Barber [14], slender pile, linear inhomogeneous soil		
$1.074 n_h^{\frac{3}{5}} (E_P I_P)^{\frac{2}{5}}$	$-0.99 n_h^{\frac{2}{5}} (E_P I_P)^{\frac{3}{5}}$	$1.48 n_h^{\frac{1}{5}} (E_P I_P)^{\frac{4}{5}}$
Gazetas [39] and Eurocode 8 Part 5 [37], slender pile, homogeneous soil		
$1.08 D_P E_{S0} \left(\frac{E_{eq}}{E_{S0}}\right)^{0.21}$	$-0.22 D_P^2 E_{S0} \left(\frac{E_{eq}}{E_{S0}}\right)^{0.50}$	$0.16 D_P^3 E_{S0} \left(\frac{E_{eq}}{E_{S0}}\right)^{0.75}$
Gazetas[39] and Eurocode 8 Part 5 [37], slender pile, linear inhomogeneous soil		
$0.60 D_P E_{S0} \left(\frac{E_{eq}}{E_{S0}}\right)^{0.35}$	$-0.17 D_P^2 E_{S0} \left(\frac{E_{eq}}{E_{S0}}\right)^{0.60}$	$0.14 D_P^3 E_{S0} \left(\frac{E_{eq}}{E_{S0}}\right)^{0.80}$
Gazetas[39] and Eurocode 8 Part 5 [37], slender pile, parabolic inhomogeneous soil		
$0.79 D_P E_{S0} \left(\frac{E_{eq}}{E_{S0}}\right)^{0.28}$	$-0.24 D_P^2 E_{S0} \left(\frac{E_{eq}}{E_{S0}}\right)^{0.53}$	$0.15 D_P^3 E_{S0} \left(\frac{E_{eq}}{E_{S0}}\right)^{0.77}$
Shadlou and Bhattacharya [72], slender pile, homogeneous soil		
$\frac{1.45 E_{S0} D_P}{f_{(\nu s)}} \left(\frac{E_{eq}}{E_{s0}}\right)^{0.186}$	$-\frac{0.30 E_{S0} D_P^2}{f_{(\nu s)}} \left(\frac{E_{eq}}{E_{s0}}\right)^{0.50}$	$\frac{0.18 E_{S0} D_P^3}{f_{(\nu s)}} \left(\frac{E_{eq}}{E_{S0}}\right)^{0.73}$
Shadlou and Bhattacharya [72], slender pile, linear inhomogeneous soil		
$\frac{0.79 E_{S0} D_P}{f_{(\nu s)}} \left(\frac{E_{eq}}{E_{s0}}\right)^{0.34}$	$-\frac{0.26 E_{S0} D_P^2}{f_{(\nu s)}} \left(\frac{E_{eq}}{E_{S0}}\right)^{0.567}$	$\frac{0.17 E_{S0} D_P^3}{f_{(\nu s)}} \left(\frac{E_{eq}}{E_{S0}}\right)^{0.78}$
Shadlou and Bhattacharya [72], slender pile, parabolic inhomogeneous soil		
$\frac{1.02 E_{S0} D_P}{f_{(\nu s)}} \left(\frac{E_{eq}}{E_{S0}}\right)^{0.27}$	$-\frac{0.29 E_{S0} D_P^2}{f_{(\nu s)}} \left(\frac{E_{eq}}{E_{S0}}\right)^{0.52}$	$\frac{0.17 E_{S0} D_P^3}{f_{(\nu s)}} \left(\frac{E_{eq}}{E_{S0}}\right)^{0.76}$

Parameter definitions:
$E_{eq} = \frac{E_P I_P}{\frac{D_P^4 \pi}{64}}$
$f_{(\nu S)} = \frac{1+\nu_S}{1+0.75\nu_S}$ for Randolph [69] and
$f_{(\nu s)} = 1 + |\nu_s - 0.25|$ for Shadlou and Bhattacharya [72]
$\beta = \sqrt[4]{\frac{k_h D_P}{E_P I_P}}$

Table 3
Stiffness formulae by different researchers for rigid piles in various soil profiles.

K_L	K_{LR}	K_R
Poulos and Davis [66] following Barber [14], rigid pile, homogeneous soil ($n = 0$)		
$k_h D_P L_P$	$-\frac{k_h D_P L_P^2}{2}$	$\frac{k_h D_P L_P^3}{3}$
Poulos and Davis [66] following Barber [14], rigid pile, linear inhomogeneous soil ($n = 1$)		
$\frac{1}{2}L_P^2 n_h$	$-\frac{1}{3}L_P^3 n_h$	$\frac{1}{4}L_P^4 n_h$
Carter and Kulhawy [28], rigid pile, rock		
$\frac{3.15G^* D_P^{\frac{2}{3}} L_P^{\frac{1}{3}}}{1-0.28\left(\frac{2L_P}{D_P}\right)^{\frac{1}{4}}}$	$-\frac{2G^* D_P^{\frac{7}{8}} L_P^{\frac{9}{8}}}{1-0.28\left(\frac{2L_P}{D_P}\right)^{\frac{1}{4}}}$	$-\frac{4G^* D_P^{\frac{4}{3}} L_P^{\frac{5}{3}}}{1-0.28\left(\frac{2L_P}{D_P}\right)^{\frac{1}{4}}}$
Shadlou and Bhattacharya [72], rigid pile, homogeneous soil ($n = 0$)		
$\frac{3.2E_{S0}D_P}{f_{(\nu_S)}}\left(\frac{L_P}{D_P}\right)^{0.62}$	$-\frac{1.7E_{S0}D_P^2}{f_{(\nu_S)}}\left(\frac{L_P}{D_P}\right)^{1.56}$	$\frac{1.65E_{S0}D_P^3}{f_{(\nu_S)}}\left(\frac{L_P}{D_P}\right)^{2.5}$
Shadlou and Bhattacharya [72], rigid pile, linear inhomogeneous soil ($n = 1$)		
$\frac{2.35E_{S0}D_P}{f_{(\nu_S)}}\left(\frac{L_P}{D_P}\right)^{1.53}$	$-\frac{1.775E_{S0}D_P^2}{f_{(\nu_S)}}\left(\frac{L_P}{D_P}\right)^{2.5}$	$\frac{1.58E_{S0}D_P^3}{f_{(\nu_S)}}\left(\frac{L_P}{D_P}\right)^{3.45}$
Shadlou and Bhattacharya [72], rigid pile, parabolic inhomogeneous soil ($n = 1/2$)		
$\frac{2.66E_{S0}D_P}{f_{(\nu_S)}}\left(\frac{L_P}{D_P}\right)^{1.07}$	$-\frac{1.8E_{S0}D_P^2}{f_{(\nu_S)}}\left(\frac{L_P}{D_P}\right)^{2.0}$	$\frac{1.63E_{S0}D_P^3}{f_{(\nu_S)}}\left(\frac{L_P}{D_P}\right)^{3.0}$
Parameter definitions:		
$E_{eq}=\frac{E_P I_P}{\frac{D_P^4\pi}{64}}$	$f_{(\nu_S)} = 1 + \lvert\nu_S - 0.25\rvert$	$\beta = \sqrt{\frac{k_h D_P}{E_P I_P}}$

2.6. Natural frequency calculations

It is of key importance to predict the natural frequency of the offshore wind turbine–support structure–foundation system because both under and over prediction of the natural frequency may be unconservative. This is because the structure is excited in a wide frequency band from wind turbulence, waves, aerodynamic and mass imbalance loads at the rotational frequency range (1P) and blade passage and rotational sampling loads at the blade passing frequency (2P or 3P). More information on the complexity of loading of offshore wind turbine foundations can be found in Burton et al. [23]; Arany et al. [9] The importance of dynamics in foundation design is demonstrated in Bhattacharya [15], Kühn [50]; Zaaijer [78]; Bhattacharya et al. [16,17], Lombardi et al. [57], Adhikari and Bhattacharya [6,5]. Fig. 10 shows a typical wind turbine's excitations in terms of frequency content.

The natural frequency of the system shown in Fig. 8 can be estimated following Arany et al. [9]; Arany et al. [12]. This simplified methodology builds on the simple cantilever beam formula to estimate the natural frequency of the tower, and then applies modifying coefficients to take into account the flexibility of the foundation and the substructure. This is expressed as

$$f_0 = C_L C_R C_S f_{FB} \tag{63}$$

where C_L and C_R are the lateral and rotational foundation flexibility coefficients, C_S is the substructure flexibility coefficient and f_{FB} is the fixed base (cantilever) natural frequency of the tower. The fixed base natural frequency of the tower is expressed simply with the equivalent stiffness k_0 and equivalent mass m_0 of the first mode of vibration as

$$f_{FB} = \frac{1}{2\pi}\sqrt{\frac{k_0}{m_0}} = \frac{1}{2\pi}\sqrt{\frac{3E_T I_T}{L_T^3\left(m_{RNA} + \frac{33}{140}m_T\right)}} \tag{64}$$

where E_T is the Young's modulus of the tower material, I_T is the average area moment of inertia of the tower, m_T is the mass of the tower, m_{RNA} is the mass of the rotor-nacelle assembly and L_T is the length of the tower. The average area moment of inertia is calculated as

$$I_T = \frac{1}{16} t_T \pi \left(D_b^3 + D_t^3\right) \tag{65}$$

where D_b is the tower bottom diameter, D_t is the tower top diameter. The average wall thickness and the average tower diameter are given by Eq. (60).

$$t_T = \frac{m_T}{\rho_T L_T D_T \pi} D_T = \frac{D_b + D_t}{2} \tag{66}$$

where ρ_T is the density of the tower material (steel). The coefficients C_L and C_R are expressed in terms of the non-dimensional foundation stiffness values:

$$\eta_L = \frac{K_L L_T^3}{EI_\eta} \eta_{LR} = \frac{K_{LR} L_T^2}{EI_\eta} \eta_R = \frac{K_R L_T}{EI_\eta} \tag{67}$$

where K_L, K_{LR}, K_R are the stiffness parameters, EI_η is the equivalent bending stiffness of the tower calculated as

$$EI_\eta = E_T I_T \bullet f(q) \; where q = \frac{D_b}{D_t} f(q) = \frac{1}{3} \bullet \frac{2q^2(q-1)^3}{2q^2 lnq - 3q^2 + 4q - 1} \tag{68}$$

Using the calculated non-dimensional stiffness values the foundation flexibility coefficients are given as

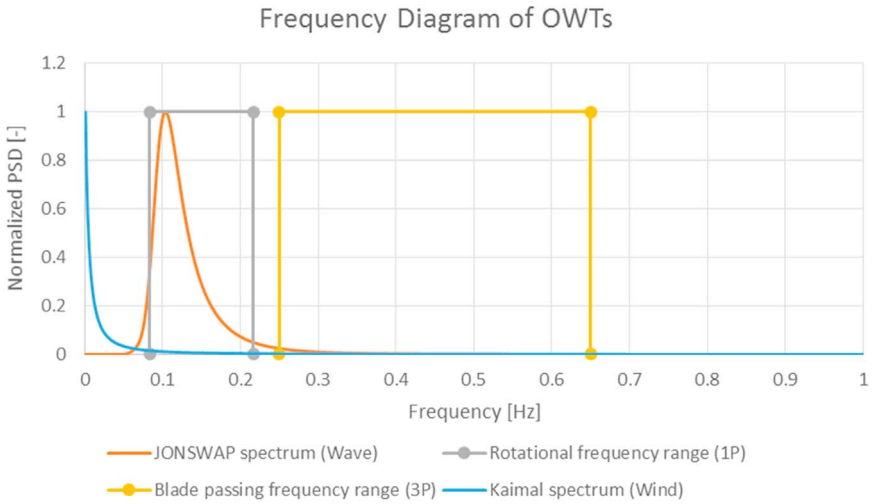

Fig. 10. Frequency content of the excitations of a typical offshore wind turbine.

$$C_R(\eta_L,\ \eta_R,\ \eta_{LR})=1-\frac{1}{1+a\left(\eta_R-\frac{\eta_{LR}^2}{\eta_L}\right)}\quad C_L(\eta_L,\ \eta_R,\ \eta_{LR})=1-\frac{1}{1+b\left(\eta_L-\frac{\eta_{LR}^2}{\eta_R}\right)} \tag{69}$$

where $a = 0.5$ and $b = 0.6$ are empirical coefficients [10]. The sub-structure flexibility coefficient is calculated by assuming that the monopile goes up to the bottom of the tower. The distance between the mudline and the bottom of the tower is L_S, and $E_P I_P$ is the bending stiffness of the monopile. The foundation flexibility is expressed in terms of two dimensionless parameters, the bending stiffness ratio χ and the length ratio ψ

$$\chi=\frac{E_T I_T}{E_P I_P}\psi=\frac{L_S}{L_T}C_S=\sqrt{\frac{1}{1+(1+\psi)^3\chi-\chi}} \tag{70}$$

A spreadsheet can be easily used to carry out the calculations. The dynamic amplification factors for loads with frequencies close to the Eigen frequency of the structure can be determined following Section 7.10.3.6 of DNV [34].

2.7. Estimating the number of cycles of loading over the life time

One of the most challenging tasks in the analysis of the long term behaviour of offshore wind turbines is the estimation of the number of cycles of loading of different magnitudes that will have an impact on the performance. This information is necessary to predict the fatigue life of the monopile, as well as to predict the accumulated mudline deformations throughout the lifetime of the structure. To properly estimate the number of cycles at different load levels, a series of time domain simulations are necessary to statistically represent all operational states of the turbine in different environmental conditions. Rainflow counting [61] can be used to count the number of cycles from these time domain simulations. There are many other cycle counting methods available, such as peak counting, level-crossing counting, simple-range counting, range-pair counting and reservoir counting. These methods, as well as rainflow counting, are defined in [13]. Many different time domain approaches are available, however, these are beyond the scope of this paper.

As it will be shown in this section, researchers have provided simple empirical formulae for estimating the accumulated rotation, and the simple linear damage accumulation rule [62] can be used to assess the fatigue life. However, without detailed data about the wind turbine and sophisticated simulation tools, it is challenging to estimate the number of load cycles.

Soil behaviour is a function of strain level and under large strains soil behaves highly non-linearly. Loose to medium dense sands may progressively build pore water pressure and liquefy. At certain threshold strains, some soils (clayey soil) may degrade while others may compact. With episodes of low strain level and under the action of tens of millions of load cycles, some soils may increase their stiffness. Therefore, to predict the long term performance, one needs to know the corresponding wave height and wave period for maximum wave load calculation which will impose the largest moment in the foundation and the corresponding strain level. It is also necessary to estimate the number of cycles of loading that would influence the soil behaviour. Therefore, one needs to estimate the number of cycles of loading in a 3 h sea state by calculating the worst-case scenario time period of wave loading. A method to predict the number of wave cycles is shown below in Section 2.7.1. The wind load cycles are typically at a much lower frequency than waves, but conservatively it is assumed that the wind and wave act at the same frequency i.e. the frequency of the wave loading.

2.7.1. Calculation of the number of wave cycles

In this step, a simplified estimation of the extreme wave height and the corresponding wave period for a given site is explained which involves the following sub-steps:

(1) Obtain the relevant significant wave height H_S from a reliable source.
(2) Calculate the corresponding range of wave periods T_S.
(3) Calculate the number of waves in a 3 h period (N).
(4) Calculate the maximum wave height H_m.
(5) Calculate the range of wave periods corresponding to the maximum wave height T_m.

The sub-steps are shown in detail.

2.7.2. Sub-step 1. Obtain 50 year significant wave height

In absence of site measured data, one can use data from offshore drilling stations or other sea state monitoring reports. For the UK, the document “Wave mapping in UK waters”, periodically prepared for the Health and Safety Executive can be used [76]. In this document one can find nearby oil and gas stations or meteorological buoys, and estimate the 50-year significant wave height at the wind farm site from that.

2.7.3. Sub-step 2. Calculate the corresponding range of wave periods

The range of wave periods for a given wave height can be estimated following DNV-OS-J101 [34], the following formula is found in Section 3.3.4.

$$11.\ 1\sqrt{\frac{H_S}{g}}\le T\le 14.\ 3\sqrt{\frac{H_S}{g}} \tag{71}$$

Typically, the most severe wave loads (following Morrison's equation or the McCamy-Fuchs diffraction solution) are produced by the lowest wave period, and the dynamic amplification is also highest since the frequency is closest to the natural frequency of the structure. Therefore, the peak wave period is taken as

$$T_S=11.\ 1\sqrt{\frac{H_S}{g}} \tag{72}$$

2.7.4. Sub-step 3. Calculate the number of waves in a 3-h period

Typically, significant wave heights are given for a 3-h period. In other words this means that the significant wave height is calculated as the mean of the highest 1/3 of all waves. Therefore, many different wave heights occur within this 3-h period, and the highest occurring wave height is called the maximum wave height H_m. To find this, one needs to know the number of waves in the 3 h period, because the more waves there are, the higher the chance of higher waves occurring.

$$N=\frac{3hours}{T_S}=\frac{10800s}{T_S}(\approx 1000) \tag{73}$$

2.7.5. Sub-step 4. Calculate the ratio of the maximum wave height to the significant wave height

The DNV code suggests to take the mode of the distribution of the highest wave heights, and thus:

$$H_m=H_S\sqrt{\frac{1}{2}ln(N)}(\approx 1.\ 87H_S) \tag{74}$$

The maximum wave height may be taken conservatively as $H_m=2H_S$. Please note that the water depth S may limit the maximum wave height. Typically, it is assumed that the breaking limit of waves (maximum possible wave height) in water depth S is $\overline{H}_m=0.78S$. However, if the seabed has a slope, the wave may be higher than this limit, as was reported at the exposed site at Blyth [27], therefore caution should be exercised when using this limit wave height.

2.7.6. Sub-step 5. Calculate the range of wave periods corresponding to the maximum wave height

The same formulae can be used as in Sub-step 2.

$$11.1\sqrt{\frac{H_m}{g}} \le T \le 14.3\sqrt{\frac{H_m}{g}} \tag{75}$$

$$T_m = 11.1\sqrt{\frac{H_m}{g}} \tag{76}$$

The wave height and wave period combination of H_m, T_m can be used for maximum wave load calculation, incorporating dynamic amplification.

2.8. Methodologies for long term rotation estimation

To fulfil the Serviceability Limit State (SLS) requirements, the long term behaviour of monopile foundations needs to be analysed according to DNV [34]. The main concern is the accumulated rotation $\Delta\theta$ and deflection $\Delta\rho$ (or equivalently the strain accumulation) at the mudline level. Even though the analysis is required by design standards, there is no consensus on an accepted methodology to carry out this analysis. Several approaches have been proposed based on extremely simple load scenarios, such as a cyclic excitation which can be described by a mean load M_{mean}, a cyclic load magnitude $M_{amp}=M_{max}-M_{min}$ and number of cycles N (see Fig. 5 for the shape of the loading). The actual load acting on an offshore wind turbine foundation, however, is extremely complicated and it is important to highlight the complexity:

(a) The loading is not cyclic but in most cases is dynamic. Loads applied are in a very wide frequency band ranging through the orders of magnitudes between 0.001–10 Hz, which includes the first few structural natural frequencies and blade natural frequencies. It is therefore difficult to estimate the numbers of load cycles. On the other hand, the frequency may be important in the determination of accumulated tilt. Even though it seems unlikely, it is not yet clear whether any significant excess pore pressures can occur and cause dynamic effects, as pointed out in Kuo et al. [51]

(b) Some of the available methods were developed for very low number of cycles. Long and Vanneste [58] points out that implicit numerical simulations typically allow for simulation of less than 50 cycles due to the accumulation of numerical errors. Furthermore, most reported tests they analysed were also carried out for 50 cycles or less and only one test had 500 cycles. The authors suggest caution when predicting the effects of very high numbers of load cycles. The numerical investigations and laboratory tests carried out by Achmus et al. [4] and Kuo et al. [51] go up to 10,000 cycles, and tests by Byrne et al. [25] and Leblanc et al. [52] have been carried out for up to 65,000 cycles. However, these are still orders of magnitudes below the expected number of load cycles of an OWT. Cuéllar [30] has run four tests with different load scenarios for a remarkable 5 million cycles and identified qualitative behaviour of deformation accumulation for high number of cycles.

(c) The magnitude of dynamic loading also ranges from small to extreme loads with load cycles ranging from a few to a few hundred cycles of extreme loads, and from millions to hundreds of millions of cycles of low amplitude vibrations. In different states of the wind turbine different load magnitudes are expected.

(d) The loading is not either one-way or two-way, but the whole range of load regimes are present at different times throughout the lifetime of the turbine. There is also disagreement in terms of whether one-way or two-way loading is more detrimental. Long and Vanneste [58] suggest that one-way loading is the critical load scenario and two-way loading causes less accumulated strain. Achmus et al. [4] and Kuo et al. [51] also focus on one-way loading in their analysis. However, Byrne et al. [25]; Leblanc et al. [52] found that the most critical scenario is two-way loading with $M_{min}/M_{max}=-0.5$.

(e) The loading is not unidirectional, loads appear both in the along-wind (x) and cross-wind (y) directions during the operational life of the turbine, and cyclic vertical (z) loads are also present. Wind and waves are also not always collinear, causing multidirectional loading on the foundation.

(f) The nacelle always turns into the wind, which means that the along-wind (x) and cross-wind (y) directions are not fixed in a global frame of reference but are turning as the yaw angle of the rotor changes. This means that the foundation is loaded both with along-wind and cross-wind loads throughout the lifetime of the turbine in all directions.

In pile design for offshore wind turbines the p-y method is typically employed, as mentioned in Section 2.4. Long and Vanneste [58] give a good account of the research efforts into the analysis of piles under cyclic lateral loading by modified 'cyclic' p-y curves. Improved p-y curves for cyclic lateral load were developed by Reese et al. [71], O'Neill and Murchinson [64], Little and Briaud [56]. More fundamental theoretical approaches have been attempted by Swane and Poulos [73] as well as Matlock et al. [60]. As Long and Vanneste [58] points out, these methods require parameters that are typically not available from site investigation.

The simplified approach of accumulated strain is often used in literature, which is equivalent to reduction of soil stiffness. The coefficient of subgrade reaction n_h can be reduced in order to account for the effects of cyclic loading. Such approach was used by Prakash [67], Davisson [32], Davisson and Salley [33]. Broms [21] pointed out that the reduction of n_h depends on the density of the cohesionless soil. These studies suggest to reduce n_h by a fixed percentage if a certain number of load cycles (~50) are expected (30% in Davisson [32], 75% and 50% for dense and loose sand in Broms [21]).

Logarithmic expressions for permanent strains of monopiles have also been proposed by Hettler [42], Lin and Liao [54], Verdure et al. [75], Achmus et al. [4] and Li et al. [53]. Power law expressions have been proposed for monopiles by Little and Briaud [56], Long and Vanneste [58], Leblanc et al. [52], Klinkvort et al. [48], and for caissons by Zhu et al. [81] and Cox et al. [29]. Cuéllar [30] proposes a method by which three different curves are used to approximate the long term accumulation.

Some important contributions are listed below.

2.8.1. The method proposed by Little and Briaud [56]

Little and Briaud [56] proposed the simple power law expression for strain accumulation

$$\varepsilon_N = \varepsilon_1 N^m \tag{77}$$

where ε_N is the strain after N cycles, ε_1 is the strain at the first load cycle and m is a constant that expresses dependence on soil and pile parameters, installation method and loading characteristics. Achmus et al. [4] uses $m = 0.136$ for typical monopiles.

2.8.2. The method proposed by Long and Vanneste [58]

Long and Vanneste [58] provide a simple approach for calculating the degradation of the coefficient of subgrade reaction determined from the analysis of 34 different load test scenarios. The degradation is expressed as

$$n_{hN} = n_{h1} N^{-t} \tag{78}$$

where n_{hN} is the coefficient after N cycles of loading, n_{h1} is the coefficient at the first cycle, t is the degradation parameter, which can be calculated according to

$$t = 0.17 F_r F_i F_d \tag{79}$$

F_r, F_i, F_d are parameters to take into account the cyclic load ratio, pile

installation method and soil density, respectively. For a driven pile (F_i=1.0) in medium sand (F_r=1.0) under one-way loading (F_r=1.0) the degradation parameter is $t = 0.17$.

Long and Vanneste [58] emphasizes that the load tests that serve for the basis of their analysis were mostly carried out for less than 50 load cycles, with only one test going up to 500. They suggest caution when applying these results for more than 50 load cycles, making the method hard to implement for OWT foundations where load cycles in the orders of magnitudes of 10^2–10^8 are expected. Furthermore, Long and Vanneste [58] points out that the most important factor is the cyclic load ratio M_{min}/M_{max}, however, in their formulation the reduction in the coefficient of subgrade reaction is not explicitly dependent of the cyclic load magnitude.

2.8.3. The method proposed by Lin and Liao [54]

Lin and Liao [54] provide a logarithmic expression for strain accumulation:

$$\varepsilon_n=\varepsilon_1[1 + t\ln(N)] \tag{80}$$

$$t=0.032L_P\sqrt{\frac{n_h}{E_P I_P}}F_r F_i F_d \tag{81}$$

L_P is the embedded length of the pile, F_r, F_i, F_d are parameters to take into account the cyclic load ratio, pile installation method and soil density, respectively. In the basic case of a driven pile in dense sand in one-way loading $t = 0.032L_P/T$ where $T = \sqrt{(E_P I_P)/n_h}$ is the pile/soil relative stiffness ratio, with n_h being the coefficient of subgrade reaction.

Lin and Liao [54] also provide a methodology to combine loads at different load levels into a single load case for the calculation of accumulated strain. This is achieved by converting all load cycles to a single load level by the method of equivalent accumulated strains. If there are two loads, say a and b, with t_a and t_b as degradation parameters and N_a and N_b as numbers of load cycles, respectively, then

$$\varepsilon_{N(a+b)}=\varepsilon_{1b}[1 + t_b\ln(N_b^*+N_b)] \tag{82}$$

where N_b^* is the equivalent load cycle number of load a in terms of the degradation parameter t_b expressed as

$$N_b^*=e^{\frac{1}{t_b}\left[\frac{\varepsilon_{1a}}{\varepsilon_{1b}}(1+t_a\ln(N_a))-1\right]} \tag{83}$$

2.8.4. The method proposed by Achmus et al. [4]

Achmus et al. [4] and Kuo et al. [51] carried out laboratory tests and developed a numerical modelling procedure for analysing the long term mudline deformations of rigid monopiles. According to their stiffness degradation method, the increase in plastic strain due to cyclic loading can be interpreted as a decrease in the soil's Young's modulus E_S

$$\frac{\varepsilon_{p1}}{\varepsilon_{pN}}=\frac{E_{SN}}{E_{S1}} \tag{84}$$

where $\varepsilon_{pN=1}$ is the plastic strain at the first load cycle, ε_{pN} is the plastic strain at the Nth cycle, and similarly for the elastic modulus. The following semi-empirical approach for strain accumulation is used:

$$\varepsilon_n=\frac{\varepsilon_1}{(N)^{-b_1(x_c)^{b_2}}} \tag{85}$$

b_1, b_2 are model parameters, x_c is the characteristic cyclic stress ratio ranging 0–1

$$x_c=\frac{(cyclic\ stress\ ratio\ at\ loading)-(cyclic\ stress\ ratio\ at\ unloading)}{1-(cyclic\ stress\ ratio\ at\ unloading)} \tag{86}$$

Basic design charts for preliminary design are presented in Achmus et al. [4] for the pile head deflection, the rotation is only slightly touched in the paper.

2.8.5. The method proposed by Leblanc et al. [52]

Byrne et al. [25] and Leblanc et al. [52] carried out tests for rigid piles in sand to assess the long term behaviour in terms of accumulated rotation at the mudline. Their tests were carried out using two main parameters:

$$\zeta_b=\frac{M_{max}}{M_R} \tag{87}$$

which describes the magnitude of loading with respect to the static moment resisting capacity of the pile M_R. The values are between 0 and 1, and

$$\zeta_c=\frac{M_{min}}{M_{max}} \tag{88}$$

which describes the nature of the cyclic loading. Values are between −1 for pure two-way loading and 1 for static load, with 0 being the pure one-way loading.

The load tests were carried out with two different values of relative density, R_d=4% and R_d=38%. After up to 65 000 cycles of loading the accumulated tilt was found to be in the form

$$\theta_N=\theta_0+\Delta\theta(N) \tag{89}$$

$$\Delta\theta(N)=\theta_S T_b(\zeta_b,\ R_d)T_c(\zeta_c)N^{0.31} \tag{90}$$

where R_d is the relative density of sand, θ_0 is the rotation at maximum load of the first load cycle, θ_S is the pile rotation under a static load equal to the maximum cyclic load. The functions $T_b(\zeta_b,\ R_d)$ and $T_c(\zeta_c)$ are given in graphs in Leblanc et al. [52]. A piecewise linear approximation for $T_c(\zeta_c)$ can be used for simplicity

$$T_c=\begin{cases}13.71\zeta_c+13.71 & for\ -1\le\zeta_c<-0.65\\ -5.54\zeta_c+1.2 & for\ -0.65\le\zeta_c<0\\ -1.2\zeta_c+1.2 & for\ 0\le\zeta_c<1\end{cases} \tag{91}$$

Similarly, the equations for $T_b(\zeta_b,\ R_d)$ can be given for two values of R_d following Leblanc et al. [52]:

$$T_b=\begin{cases}0.4238\zeta_b-0.0217 & for\ R_d=38\%\\ 0.3087\zeta_b-0.0451 & for\ R_d=4\%\end{cases} \tag{92}$$

2.8.6. The work of Cuéllar [30]

Cuéllar [30] carried out lateral load tests of a rigid monopile, running 4 different load case scenarios for a remarkable 5 million load cycles. The goal of the analysis was to identify qualitative trends in the strain accumulation and to analyse densification of the soil due to cyclic lateral load on the pile. It was found in their study that the plot of the accumulation of permanent deformation against the number of cycles can be approximated by three different simplified curves.

(1) In the first roughly 10^4 cycles, the accumulation follows a logarithmic curve in the form of $\rho_1=C_1+C_2\log(N)$. A quick accumulation of permanent displacements likely due to the densification around the pile is followed by a region of stabilised cyclic amplitude.
(2) Stabilised cyclic amplitude is characteristic of this intermediate region where the accumulation is roughly linear with $\rho_2=C_3+C_4N$.
(3) The last section after the second inflection point at roughly 10^6 number of cycles can be approximated by a power law curve as $\rho_3=C_5N^{C_6}$.

The rate of accumulation never seems to fall to zero, the accumulated rotation appears to increase indefinitely.

2.9. Methodology for fatigue life estimation

The analysis of fatigue life of the substructure has to be carried out, which is typically done following DNV-RP-C203- "Fatigue design of offshore steel structures" [35]. This paper is aimed at providing a simple methodology for the conceptual design of monopiles, and therefore fatigue life issues related to other components of the substructure (e.g. transition piece, grouted connection, J-tubes, etc) are naturally omitted. In terms of fatigue analysis of the structural steel of the pile wall under bending moment, one has to calculate the stress levels caused by the load cases in Table 1. The material factor γ_M=1.1 and load factor γ_L=1.0 are used, following [34]. With these the maximum stress levels σ_m caused by the load cases can be calculated as

$$\sigma_m=\gamma_L M_{max}\frac{D_P}{2I_P} \tag{93}$$

where M_{max} is the maximum bending moment that occurs in the given load case, D_P and I_P are the pile diameter and area moment of inertia, respectively. The maximum cyclic stress amplitude is given as

$$\sigma_c=\gamma_L\frac{(M_{max}-M_{min})}{2}\frac{D_P}{2I_P} \tag{94}$$

where M_{min} is the lowest bending moment occurring in each load case.

In typical practical cases, the fatigue analysis of the structural steel of a monopile results in sufficient fatigue life with a high margin. However, the welds of flush ground monopiles are more prone to fatigue type failure as fatigue crack initiation typically occurs around the welds before it would occur in the structural steel. The fatigue analysis of welds of flush ground monopiles is carried out using the C1 and D classes defined in DNV [35]. A thickness correction factor has to be applied as monopile welds are almost always thicker than 25 mm. These curves build on tests carried out specifically for the requirements of the offshore oil and gas industry. Currently research and testing is ongoing in the SLIC Joint Industry Project [20] to develop S-N curves representative of the load regime, geometry, materials, environmental conditions and manufacturing procedures of the offshore wind industry.

More detailed fatigue analyses through e.g. finite element analysis may need to be carried out once a more detailed design is available, as fatigue type failure is expected to occur in weak points in the structure (e.g. holes, welds and joints) where stress concentration is expected and crack initiation is more likely. Furthermore, a crack propagation approach is generally more suitable for detailed fatigue design and simple S-N curve fatigue analyses are often not satisfactory to predict the fatigue life of certain structural details.

3. Worked example: design steps using a typical site from the UK

A site is considered from the outer Thames Estuary (Eastern Coast of the UK) and the chosen turbine is Siemens SWT-3.6-120. The site is a shallow water site with water depth ranging from intertidal (occasionally no water) to 25 m mean water depth. Depending on the location of the WTG within the wind farm, several different pile designs are required. In this example the deepest water (25 m) is considered. The turbine is at the edge of the wind farm, and fatigue loads due to turbulence generated by other turbines is neglected in this analysis. The soil at the site is predominantly London clay with sands and gravels in the uppermost layers. This section of the paper considers the application of the simplified design procedure:

3.1. Establishing design criteria

The design criteria are typically established based on:

(a) Design codes: the most important ones are design requirements by IEC defined in IEC-61400-1 [44], IEC-61400-3 [45], DNV-OS-J101 'Design of Offshore Wind Turbine Structures' [34] and the Germanischer Lloyd Windenergie's 'Guideline for the Certification of Offshore Wind Turbines' (Germanischer Lloyd [40]). For fatigue analyses, DNV-RP-C203 'Fatigue design of offshore steel structures' [35] is relevant. For the assessment of environmental conditions DNV-RP-C205 'Environmental conditions and environmental loads' [36] may need to be consulted. The API code of practice 'Recommended Practice for Planning, Designing and Constructing Fixed Offshore Platforms – Working Stress Design' [7] may be relevant.
(b) Certification body: typically a certification body allows for departure from the design guidelines if the design is supported by sound engineering and sufficient evidence/test results.
(c) Client: occasionally the Client may pose additional requirements based on their appointed consultant.
(d) Turbine manufacturer: the manufacturer of the wind turbine typically imposes strict Serviceability Limit State (SLS) requirements. In addition, the expected hub height is also a requirement for the turbine type and the site. The tower dimensions are also often inputs to foundation design.

The requirements are summarized in Table 4.

3.2. Obtain input data

This simplified analysis aims to use minimal amount of information about the turbine and the site, in order to enable the designer of monopiles to find the necessary pile dimensions quickly and easily for feasibility studies, tender design and early design phases. The necessary data are given below by data groups.

3.2.1. Basic turbine data

The basic turbine data required for these analyses are listed in Table 5. They are typically obtained from the manufacturer of the turbine, however, a large portion of the data can be found in brochures and online databases, such as 4COffshore.com [3] or LORC.dk [55].

3.2.2. Metocean data

The most important Metocean data for this simplified analysis are summarized in Table 6. These are wind speed and turbulence characteristics, wave characteristics, water depth at the site and maximum current speed at the site. These data are typically obtained from measurements, either at the site or close to the site location, taken over many months or even several years. The wind speed data are of key importance for the estimation of energy production potential (and thus the profitability) of the offshore wind farm, and is typically readily available by the time the design of the wind farm starts. Wave data can be obtained from measurement data by government agencies, as well as from oil and gas production stations (see e.g. Williams [76]). The relevant data for the example site for the current simplified analysis are given in Table 6.

3.2.3. Geological and geotechnical data

The geological and geotechnical data are the most challenging as well as expensive to obtain and require site investigation. A good source of information is the British Geological Survey, which contains data from around the UK. In the worst case scenario, a first estimation can be carried out by just knowing the basic site classification such as stiff clay or dense sand.

The geotechnical data necessary for the analysis include:

(1) Ground profile: For the example site, it is assumed that the uppermost layers (roughly the upper 20 m) are loose to medium dense sand and silt overlying layers of London clay.
(2) Strength and stiffness parameters: Loose to medium sand/silt in

Table 4
Design basis or criteria for design.

#		Category	Description	Limit
R1	R1.A	ULS	Foundation's load carrying capacity has to exceed the maximum load (for horizontal and vertical load, and overturning moment).	$M_{ULS} < M_f$ $F_{ULS} < F_f$ $V_{ULS} < V_f$
	R1.B	ULS	The pile's yield strength should exceed the maximum stress.	$\sigma_m < f_{yk}$
	R1.C	ULS	Global (Euler type or column) buckling has to be avoided.	
	R1.D	ULS	Local (shell) buckling has to be avoided.	
R2		FLS	The lifetime of the foundation should be at least 50 years.	$T_L > 50yrs$
R3	R3.A	SLS	Initial deflection must be less than 0.2 m.	$\rho_0 < 0.2m$
	R3.B	SLS	Initial tilt must be less than 0.5°.	$\theta_0 < 0.5°$
	R3.C	SLS	Accumulated deflection must be less than 0.2 m.	$\rho_{acc} < 0.2m$
	R3.D	SLS	Accumulated tilt must be less than 0.25°.	$\theta_{acc} < 0.25$
R4		SLS (Natural frequency)	The structural natural frequency of the wind turbine-tower-substructure-foundation system has to avoid the frequency of rotation of the rotor (1P) by at least 10%.	$f_0 > 1.1 f_{1P,max} = 0.24$Hz
R5		Installation	Pile wall thickness (initial guess)	$t_P \geq 6.35 + \frac{D_P}{100}$ [mm]

Table 5
Turbine data and chosen pile material parameters.

Parameter	Symbol	Value	Unit
Hub height	z_{hub}	87	m
Rotor diameter	D	120	m
Tower height	L_T	68	m
Tower top diameter	D_t	3	m
Tower bottom diameter	D_b	5	m
Tower wall thickness	t_T	0.027	m
Density of the tower material	ρ_T	7860	kg/m^3
Tower mass	m_T	250	tons
Rated wind speed	U_R	12	m/s
Mass of the rotor-nacelle assembly (RNA)	m_{RNA}	243	tons
Operational rotational speed range of the turbine	Ω	5–13	rpm

Table 6
Metocean data.

Parameter	Symbol	Value	Unit
Wind speed Weibull distribution shape parameter	s	1.8	[-]
Wind speed Weibull distribution scale parameter	K	8	m/s
Reference turbulence intensity	I	18	%
Turbulence integral length scale	L_k	340.2	m
Density of air	ρ_a	1.225	kg/m^3
Significant wave height with 50-year return period	H_S	6.6	m
Peak wave period	T_S	9.1	s
Maximum wave height (50-year)	H_m	12.4	m
Maximum wave peak period	T_m	12.5	s
Maximum water depth (50-year high water level)	S	25	m
Density of sea water	ρ_w	1030	kg/m^3

the upper layers have a submerged unit weight of $\gamma'=9$[kN/m^3] and the friction angle in the range of $\phi'=28-36°$.

The modulus of subgrade reaction is chosen following Terzaghi [74]. The soil's modulus of subgrade reaction is approximated as linearly increasing, with coefficient of subgrade reaction

$$n_h = \frac{A \bullet \gamma'}{1.35} \approx \frac{600 \bullet 9000}{1.35} = 4 \left[\frac{\text{MN}}{\text{m}^3}\right] \tag{95}$$

where $A = 300-1000$ for medium dense sand and $A = 100-300$ for loose sand, $\gamma'=9$[kN/m^3] as given above. The geotechnical data are summarized in Table 7.

3.2.4. Pile and transition piece

The pile's material is chosen as the industry standard S355 structural steel. The important properties of this material is the Young's modulus E_P, the density ρ_P and the yield strength f_{yk}, which are given in Table 7. The use of higher strength steel may be considered for foundation design, however, cost constraints typically result in S355 being used. The total width of the grout and the transition piece together is taken as $t_{TP}+t_G=0.15$[m], which results in the substructure diameter.

3.3. Guess initial pile dimensions

The initial pile dimensions are guessed based on the Ultimate Limit State (ULS) design load. The load calculations are carried out following Arany et al. [11] and a spreadsheet can be used to carry out these calculations. The wind load on the rotor can already be calculated in the first step, however, the wave loading depends on the monopile diameter, and therefore it can only be calculated after the initial pile dimensions are available.

3.3.1. Calculate highest wind load

The wind load for ULS is determined from the 50-year Extreme Operating Gust (EOG), which is assumed to produce the highest single occurrence wind load, this is wind scenario (U-3) in Section 2.2.1. The procedure outlined in Section 2.2.2 is used to estimate the wind load for this scenario. First the EOG wind speed is calculated using data from Tables 5 and 6.

$$U_{10,50-year} = 35.7 \left[\frac{\text{m}}{\text{s}}\right] U_{10,1-year} = 28.6 \left[\frac{\text{m}}{\text{s}}\right] \sigma_{U,c} = 3.15 \left[\frac{\text{m}}{\text{s}}\right] u_{EOG} = 8.1 \text{[m/s]} \tag{96}$$

Using this the total load wind load is estimated as

$$Th_{wind,EOG} \approx 1.63 \text{[MN]} \tag{97}$$

and using the water depth $S = 25[m]$ and the hub height above mean sea level $z_{hub}=87$[m]

$$M_{wind,EOG} = Th_{wind,EOG}(S + z_{hub}) \approx 182 \text{[MNm]} \tag{98}$$

Applying a load factor of $\gamma_L=1.35$ the total wind moment is ~246[MNm]. Calculation of the wind load for the other load cases is omitted here for brevity, however, it is found that the EOG at U_R (U-3) gives the highest load.

3.3.2. Calculate initial pile dimensions

Using the pile thickness formula of API [7] given in Eq. 1, the following can be written for the area moment of inertia of the pile cross section

$$I_P = \frac{1}{8}(D_P - t_P)^3 t_P \pi = \frac{1}{8}\left(D_P - 6.35 - \frac{D_P}{100}\right)^3 \left(6.35 + \frac{D_P}{100}\right)\pi \tag{99}$$

Table 7
Geotechnical, pile material and transition piece data.

Parameter	Symbol	Value	Unit
Soil's submerged unit weight	γ'	9	kN/m^3
Soil's angle of internal friction	ϕ'	28–36	°
Soil's coefficient of subgrade reaction	n_h	4000	kN/m^3
Pile wall material – S355 steel – Young's modulus	E_P	200	GPa
Pile wall material – S355 steel – density	ρ_P	7860	kg/m^3
Pile wall material – S355 steel – Yield stress	f_{yk}	355	MPa
Grout and transition piece combined thickness	t_G+t_{TP}	0.15	[m]

The following has to be satisfied to avoid pile yield with material factor γ_M=1.1

$$\sigma_m=\frac{M_{wind,EOG}}{I_P}\frac{D_P}{2}<\frac{f_{yk}}{\gamma_M}\approx 322\,[\text{MPa}] \tag{100}$$

from which the required diameter is determined as

$$\frac{D_P}{I_P}<\frac{2f_{yk}}{\gamma_M M_{wind,EOG}} \tag{101}$$

This results in an initial pile diameter of D_P=4.6[m] with a wall thickness of $t_P\approx$53[mm].

The embedded length is determined next. The formula of Poulos and Davis [66] given in Eq. (6) can be used to estimate the required embedded length

$$L_P=4.0\left(\frac{E_P I_P}{n_h}\right)^{\frac{1}{5}}\approx 39\,[\text{m}] \tag{102}$$

The initial pile dimensions are then

$$D_P=4.5\,[\text{m}]\ t_P=0.051\,[\text{m}]\ L_P=39\,[\text{m}] \tag{103}$$

3.4. Estimate loads on the foundation

Now that an initial guess for the pile dimensions is available, the wave load can be calculated. For the combination of wind and wave loading, many load cases are presented in design standards. Five conservative load cases are considered in Table 1. One of the potential severe load cases not covered by these scenarios are shutdown events of the wind turbine, as these situations require detailed data about the wind turbine (rotor, blades, control system parameters, generator, etc), but are likely to provide a lower foundation load than the scenarios in Table 1.

3.4.1. Calculate wind loads (other wind scenarios)

The wind loads on the structure are independent of the substructure diameter, and therefore the wind loads can be evaluated before the pile and substructure design is available. Section 2.2.2 is used to determine the turbulent wind speed component and through that the thrust force and overturning moment, following Eqs. (10)–(24). Table 8 summarizes the important parameters and presents the wind loads for the different wind scenarios. Note that the mean of the maximum and minimum loads is not equal to the mean force without turbulent wind component. This is because the thrust force is proportional to the square of the wind speed (see Eq. (10)).

3.4.2. Calculate critical wave loads

The wave load is first calculated only for the most severe wave scenarios used for Load Cases E-2 and E-3, that is, wave scenario (W-2) and (W-4), the 1-year and 50-year Extreme Wave Heights (EWH). The methodology described in Section 2.2.3 is used to calculate the wave loading, and Eq. 9 is used to calculate the substructure diameter, which in this case is D_S=4.8[m]. The relevant 50-year wave height and wave period are taken from Table 6. The 1-year equivalents are calculated following [34] from the 50-year significant wave height according to

$$H_{S,1}=0.8H_{S,50}=5.3\,[\text{m}]\ T_{S,1}=11.1\sqrt{H_{S,1}/g}=8.1\,[\text{s}] \tag{104}$$

and then the procedure in Section 2.7.1 is used to determine the 1-year maximum wave height and period,

$$H_{m,1}=10.1\,[\text{m}] \text{ and } T_{m,1}=11.2\,[\text{s}] \tag{105}$$

The wave heights and wave periods are summarized for all wave scenarios (W-1)–(W-4) in Table 9.

The maximum of the inertia load occurs at the time instant t = 0 when the surface elevation η = 0 and the maximum of the drag load occurs when $t = T_m/4$ and $\eta = H_m/2$.

The maximum drag and inertia loads for wave scenario (W-2) with the 1-year EWH are then

$$F_{D,max}=0.65\,[\text{MN}]\ M_{D,max}=17.1\,[\text{MNm}]\ F_{I,max}=1.48\,[\text{MN}]\ M_{I,max}=36.7\,[\text{MNm}] \tag{106}$$

The maxima of the wave loads and moments may be conservatively taken as

$$F_{wave,W-2}=2.13\,[\text{MN}] \text{ and } M_{wave,W-2}=53.8\,[\text{MNm}]$$

Similarly, for the 50-year EWH in wave scenario (W-4) the drag and inertia loads are given as

$$F_{D,max}=1.07\,[\text{MN}]\ M_{D,max}=23.8\,[\text{MNm}]\ F_{I,max}=1.7\,[\text{MN}]\ M_{I,max}=43.9\,[\text{MNm}] \tag{107}$$

and the maxima of the wave load

$$F_{wave,W-4}=2.77\,[\text{MN}]\ M_{wave,W-4}=67.7\,[\text{MNm}] \tag{108}$$

3.4.3. Load combinations for ULS

The most severe load cases in Table 1 for ULS design are E-2 and E-3, the extreme wave scenario (50-year EWH) combined with Extreme Turbulence Model (ETM) and the extreme operational gust (EOG) combined with the yearly maximum wave height (1-year EWH). A

Table 8
Load and overturning moment for wind scenarios (U-1)–(U-4).

Parameters	Symbol [unit]	Wind scenario (U-1)	Wind scenario (U-2)	Wind scenario (U-3)	Wind scenario (U-4)
Standard deviation of wind speed	σ_U [m/s]	2.63	3.96	–	–
Standard deviation in f>f$_{1P}$	$\sigma_{U,f>f_{1P}}$[m/s]	0.73	1.22	–	–
Turbulent wind speed component	u [m/s]	0.94	2.44	8.1	4.86
Maximum force in load cycle	F$_{max}$ [MN]	0.68	0.84	1.63	0.40
Minimum force in load cycle	F$_{min}$ [MN]	0.49	0.37	0.39	0.25
Mean force without turbulence	F$_{mean}$ [MN]	0.58	0.58	0.58	0.28
Maximum moment in load cycle	M$_{max}$ [MN]	75.8	94.4	182.8	44.6
Minimum moment in load cycle	M$_{min}$ [MN]	55.4	41.4	43.7	28.1
Mean moment without turbulence	M$_{mean}$ [MN]	65.2	65.2	65.2	31.3

Table 9
Wave heights and wave periods for different wave scenarios.

Parameters	Symbol [unit]	Wave scenario (W-1)	Wave scenario (W-2)	Wave scenario (W-3)	Wave scenario (W-4)
Wave height	H [m]	5.3	10	6.6	12.4
Wave period	T [s]	8.1	11.2	9.1	12.5

partial load factor of γ_L=1.35 has to be applied for ULS environmental loads according to DNV [34] and IEC (2009). Table 10 shows the ULS loads for the two load combinations, and it is clear from the table that for this particular example the driving scenario is (E-3) since the overturning moment is dominated by the wind load.

The new total loads in Table 10 are used to recalculate the required foundation dimensions following Section 3.3.2. This will result in an iterative process of finding the necessary monopile size for the ULS load, which can be easily solved in a spreadsheet. The analysis results in the following dimensions:

$$D_P=4.\,9[\mathrm{m}]\ t_P=56[\mathrm{mm}]\ L_P=42[\mathrm{m}] \tag{108}$$

The stability analysis has to be carried out following Germanischer Lloyd [40] Chapter 6 on the design of steel support structures.

3.5. Estimate geotechnical load carrying capacity

In typical scenarios, the limiting case for maximum lateral load results from the yield strength of the pile. However, a check has to be performed to make sure that the foundation can take the load, that is, that the soil does not fail at the ULS load. Following equations of Section 2.3.2, the ultimate horizontal load bearing capacity and the ultimate moment capacity of the pile are established as F_R=38MN and M_R=2275MNm, respectively. These are well above the limit.

In terms of vertical load, it is expected that failure due to lateral load occurs first and that stability under lateral load ensures the pile's ability to take the vertical load imposed mainly by the deadweight of the structure. The analysis of vertical load carrying capacity is therefore omitted here, but has to be performed in actual design.

3.6. Estimate deformations and foundation stiffness

The foundation stiffness is estimated following Poulos and Davis [66], as it was found to be the most reliable approach for natural frequency estimation. The method requires the modulus of subgrade reaction for cohesive (clayey) and the coefficient of subgrade reaction for cohesionless (sandy) soils. The upper layers are dominant for the calculation of deflections and stiffness. The sand and silt layers were approximated here with the coefficient of subgrade reaction n_h=4[MN/m^3] following Terzaghi [74], see Eq. (95). The foundation stiffnesses are calculated using the Poulos & Davis [66] formulae for flexible piles in medium sand from Table 2 as

$$K_L=1.\,074n_h^{\frac{3}{5}}(E_PI_P)^{\frac{2}{5}}\ K_{LR}=-0.\,99n_h^{\frac{2}{5}}(E_PI_P)^{\frac{3}{5}}\ K_R=1.\,48n_h^{\frac{1}{5}}(E_PI_P)^{\frac{4}{5}} \tag{109}$$

and their values are

$$K_L=0.\,57\left[\frac{\mathrm{GN}}{\mathrm{m}}\right]K_{LR}=-5.\,9[\mathrm{GN}]\ K_R=99.\,3[\mathrm{GN/rad}] \tag{110}$$

The deflections and rotations are calculated following Eqs. 61 and 62

$$\rho=10.\,4[cm]\ \theta=0.\,569[^\circ] \tag{110}$$

The pile tip deflection is acceptable but the rotation exceeds 0.5°.

Again, an iterative process is necessary by which the necessary pile dimensions are obtained. This can be done by the following iterative steps:

Table 10
ULS load combinations.

Load	Extreme Wave Scenario (E-2) ETM (U-2) and 50-year EWH (W-4)	Extreme Wind Scenario (E-3) EOG at U_R (U-3) and 1-year EWH (W-2)
Maximum wind load [MN]	0.84	1.63
Maximum wind moment [MNm]	94.4	182.6
Maximum wave load [MN]	2.77	2.13
Maximum wave moment [MNm]	67.7	53.8
Total load [MN]	3.61	3.79
Total overturning moment [MNm]	162.1	236.4

(1) the foundation dimensions are increased following Sections 2.1 and 3.3.2,
(2) recalculate the foundation loads following Section 2.2.
(3) the foundation stiffness parameters are recalculated following Eq. (109).
(4) the mudline deformations are recalculated following Eqs. (61) and (62).
(5) the process is repeated until the deflection and rotation are both below the allowed limit.

A spreadsheet can be used to easily obtain the necessary dimensions as

$$D_P=5.\,2[m]t_P=59[mm]\ L_P=43[m] \tag{112}$$

and the deformations are now

$$\rho_0=0.\,095[m]\ \theta_0=0.\,495[^\circ] \tag{113}$$

3.7. Calculate natural frequency and dynamic amplification factors

The natural frequency is calculated following Arany et al. [8] and Arany et al. [12], as shown in Section 2.6. The first natural frequency and the damping of the first mode in the along-wind and cross-wind directions are used to obtain the dynamic amplification factors (DAF) that affect the structural response.

3.7.1. Calculate natural frequency

The structural natural frequency of the turbine-tower-substructure-foundation system is given in Eq. (63) as $f_0=C_LC_RC_Sf_{FB}$, where C_S, C_R and C_L are the substructure flexibility coefficient and the rotational and lateral foundation flexibility coefficients, respectively. The fixed base natural frequency is

$$f_{FB}=\frac{1}{2\pi}\sqrt{\frac{3E_TI_T}{L_T^3(m_{RNA}+\frac{33}{140}m_T)}}=0.\,379[\mathrm{Hz}] \tag{114}$$

The substructure flexibility coefficient C_S is calculated by assuming that the monopile goes up to the bottom of the tower. The tower is 68 m tall, the hub height is 87 m, the nacelle is ~5 m tall, so the distance between the mudline and the bottom of the tower is about L_S=41.5[m] (this is the platform height as given in Section 2.1.4). The foundation flexibility is expressed in terms of two dimensionless parameters, the bending stiffness ratio $\chi = E_TI_T/(E_PI_P) = 0.214$ and the length ratio $\psi = L_S/L_T$=0.6104.

$$C_S=\sqrt{\frac{1}{1+(1+\psi)^3\chi-\chi}}=0.\,773 \tag{115}$$

The nondimensional foundation stiffnesses are calculated based on Eqs. (67) and (68) as

$$\eta_L=\frac{K_L L_T^3}{EI_\eta}=978\ \eta_{LR}=\frac{K_{LR}L_T^2}{EI_\eta}=-149\ \eta_R=\frac{K_R L_T}{EI_\eta}=36.9 \tag{116}$$

and the foundation flexibility coefficients are calculated from these following Eq. (69) as

$$C_R=1-\frac{1}{1+0.6\left(\eta_R-\frac{\eta_{LR}^2}{\eta_L}\right)}=0.895$$
$$C_L=1-\frac{1}{1+0.5\left(\eta_L-\frac{\eta_{LR}^2}{\eta_R}\right)}=0.995 \tag{117}$$

The natural frequency is then

$$f_0=0.995\bullet 0.895\bullet 0.773\bullet 0.379=0.6884\bullet f_{FB}=0.261\,[\mathrm{Hz}] \tag{118}$$

This is acceptable, as the condition was that $f_0>0.24$[Hz].

3.7.2. Calculate dynamic amplification factors

The dynamic amplification of the wave loading is calculated using the peak wave frequency and an assumed damping ratio. The total damping ratios for the along-wind (x) and cross-wind (y) directions are chosen conservatively as 3% and 1%, respectively. The along-wind damping is larger due to the significant contribution of aerodynamic damping. In real cases the aerodynamic damping depends on the wind speed, and the along-wind value may be between 2–10%. The chosen value is conservatively small for the relevant wind speed ranges, see e.g. Camp et al. [27], or the discussion on damping in Arany et al [12]. The dynamic amplification factors are calculated as

$$DAF=\frac{1}{\sqrt{\left(1-\left(\frac{f}{f_0}\right)^2\right)^2+\left(2\xi\frac{f}{f_0}\right)^2}} \tag{119}$$

where f is the excitation frequency, f_0 is the Eigen frequency and ξ is the damping ratio. The DAFs for all wave scenarios are presented in Table 11. The difference in DAFs in the along-wind (x) and cross-wind (y) directions is apparently negligible for this example, and in Table 11 the higher value is used when loads with DAF are calculated.

3.7.3. Recalculate wave loads and foundation dimensions

The ultimate load case and the deformations have to be checked again to include dynamic amplification of loads. The wave loads recalculated for the increased pile diameter given in Eq. (112) are presented in Table 11. The updated values of foundation dimensions are obtained through an iterative process as before, easily calculable in a spreadsheet. The final dimensions are

$$D_P=5.2[m]\ t_P=59[mm]\ L_P=43[m]\ f_0=0.261[Hz] \tag{120}$$

The final loads for each load scenario (E-1) to (E-4) are given in Table 12, using data from Tables 8 and 11. The table also contains the maximum stresses and cyclic stress amplitudes for each load case.

3.8. Long term natural frequency change

The dynamic stability of the structure can be threatened by changing structural natural frequency over the lifetime of the turbine. Resonance may occur with environmental and mechanical loads resulting in catastrophic collapse or reduced fatigue life and serviceability. Therefore, it is an important aspect to see the effects of changing soil stiffness on the natural frequency of the structure. Fig. 11 shows the percentage change in natural frequency against the percentage change in the soil stiffness (coefficient of subgrade reaction n_h). It can be seen from the figure that a change of 30% in soil stiffness produces less that 1.5% change in the natural frequency. It is also apparent that degradation is more critical than stiffening from the point of view of frequency change.

3.9. Long term deflection and rotation

The rotation prediction is typically the critical aspect in monopile design as opposed to the prediction of deflection. An attempt has been made to use the method of Leblanc et al. [52] for the prediction of the long term tilt. In addition to problems listed in Section 2.8 another practical problem occurs when using this approach. Leblanc et al. [52] investigated the ultimate moment capacity of the pile by experiments and noted that a clear point of failure could not be established from the tests, and thus they defined the ultimate moment capacity – somewhat arbitrarily – as the bending moment that causes 4° of mudline rotation. However, this value was found to be relatively close to the value calculated by the method given in Section 2.3 following Poulos and Davis [66]. The approach of Poulos and Davis [66] gave the ultimate moment capacity as $M_{R,P-D}=2275$[MNm] while the 4° rotation approach gave $M_{R,4^\circ}=2029$[MNm] based on linearity of K_R value given in Table 2. Note that both these values are significantly higher than the maximum moment that is expected ($M_{ULS}=261.7$[MNm], and also than the pile yield bending moment $M_f\approx 390$[MNm].

The tests carried out by Leblanc et al. [52] for rigid piles utilize relatively high levels of loading to establish the long term rotation as a function of the number of cycles. This is likely due to the high levels of ultimate moment capacity $M_{R,4^\circ}$ estimated by their approach as compared to typical pile yield failure limits M_f. This resulted in test scenarios with significantly higher levels of loading than those expected for an actual offshore wind turbine. The test scenarios have been carried out with maximum load magnitude to load capacity ratios $\zeta_b=M_{max}/M_R$ between 0.2 and 0.53 for a relative density of $R_d=4\%$, and between 0.27 and 0.52 for the relative density of $R_d=38\%$. A linear curve has been fitted to the test results by Leblanc et al. [52] in a graph, and approximate equations have been given in this paper in Section 2.8.5. Using these linear expressions, the test results can be extrapolated beyond the range of measured results. However, the linear equations cross the abscissa at ~0.15 and ~0.06 for $R_d=4\%$ and $R_d=38\%$, respectively, and below these values the equation takes negative values, which is unrealistic. This is shown in Fig. 12.

Using the maximum bending moments calculated conservatively in Table 10 for the design load cases defined in Table 1, the ratio is only

Table 11
Dynamic amplification factors and wave loads.

Parameters	Symbol [unit]	Wave scenario (W-1)	Wave scenario (W-2)	Wave scenario (W-3)	Wave scenario (W-4)
Wave period	T [s]	8.1	11.2	9.1	12.5
Wave frequency	f [Hz]	0.123	0.089	0.110	0.080
Dynamic amplification – along-wind	DAF_x [-]	1.285	1.131	1.215	1.103
Dynamic amplification – cross-wind	DAF_y [-]	1.288	1.133	1.215	1.104
Total wave load	F_w [MN]	1.41	2.77	1.77	3.56
Total wave moment	M_w [MNm]	32.1	69.8	40.0	97.2
Total wave load with DAF	$F_{w,DAF}$ [MN]	1.82	3.14	2.15	3.93
Total wave moment with DAF	$M_{w,DAF}$[MNm]	41.4	79.1	48.6	107.3

Table 12
Calculated loads with dynamic amplification factors.

Parameter	Normal operation E-1	Extreme wave scenario E-2	Extreme wind scenario E-3	Cut-out wind+extreme wave E-4	Wind-wave misalignment E-5
Mean wind load [MNm]	65.2	65.2	65.2	31.2	65.2
Maximum wind load [MNm]	75.8	94.4	182.6	44.6	94.4
Minimum wind load [MNm]	55.4	30.7	43.7	28.1	30.7
Maximum wave load [MNm]	41.4	107.3	79.1	107.3	107.3
Minimum wave load [MNm]	−41.4	−107.3	−79.1	−107.3	−107.3
Combined maximum load [MNm]	117.2	201.7	261.7	151.9	142.9
Combined minimum load [MNm]	14	−76.6	−35.4	−79.2	30.7
Cycle time period [s]	8.1	12.5	11.2	12.5	12.5
Cycle frequency [Hz]	0.123	0.080	0.089	0.080	0.080
Maximum stress level [MPa]	96.8	166.6	216.1	125.5	166.6
Maximum cyclic stress amplitude [MPa]	131.0	255.2	281.5	214.1	255.2

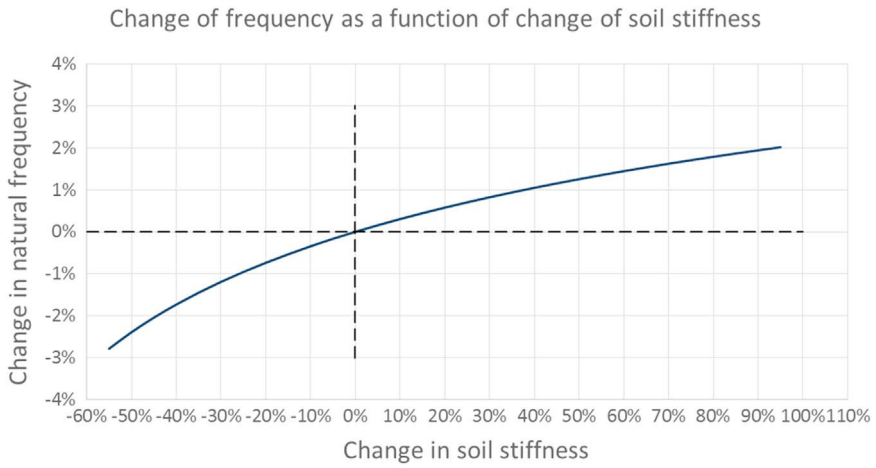

Fig. 11. Frequency change due to change in soil stiffness during the lifetime of the turbine.

ζ_b=0.13 even for the most severe 50-year maximum ULS load M_{ULS}=261.7[MNm], which is expected to occur only once in the lifetime of the turbine. The soil's angle of internal friction in the chosen site is about 28-36°, with the average in the upper regions being around 30°, therefore the R_d=4% curve is assumed to be more representative. It is clear from Fig. 12 that the actual load magnitudes expected throughout the lifetime of the turbine are in the range where the linear extrapolation of the test results of Leblanc et al. [52] would give unrealistic negative values for the rotation accumulation. Most of the likely lifetime load cycles for typical turbines would have magnitudes in the region below the range of available scale test results (i.e. ζ_b<0.15).

It is clear that it is hard to arrive at a conclusion about the accumulation of pile head rotation following this method when the expected load cycle magnitudes in practical problems are below the lower limit of the scale tests. Guidance is not given regarding these load scenarios in Leblanc et al. [52], and it is not known whether it is safe to assume no rotation accumulation below the point where the linear approximation curve reaches zero (i.e below ~0.15 for R_d=4% and below ~0.06 for R_d=38%). The methodology cannot be used for such scenarios due to a lack of data for relevant load levels.

If the load levels predicted are out of range, it is suggested to complement this analysis with the calculation of relevant strain levels in the soil due to the pile deformation. The long term behaviour can then be based on the maximum strain levels expected for the type of soils at the site. Resonant Column test or Cyclic simple shear test or Cyclic Triaxial test of soil samples can be carried out to predict the long term behaviour using the concept of threshold strain, see Lombardi et al. [57] for monopiles in cohesive soils.

3.10. Fatigue life

The fatigue analysis of the structural steel and the weld of the flush ground monopile is carried out using the methodology described in Section 2.9. Material factor of γ_M=1.1 is used and the yield strength of the S355 structural steel used for the monopile is thus reduced to σ_y=322[MPa]. A load factor of γ_L=1.0 is applied. With these the maximum stress levels caused by the load cases can be calculated following Section 2.9 and the results are given in Table 12. It was found that the highest stress amplitude observed is $\sigma_{m,max}$=216.1[MPa] and the maximum cyclic stress amplitude is $\sigma_{c,max}$=281.5[MPa]. In a study by Kucharczyk et al. [49] it was identified that the fatigue endurance limit of the S355 steel is σ_{end}=260[MPa]. Fatigue endurance limit of the material means that under stress cycles with a magnitude lower than this value, the material can theoretically withstand any number of cycles. The highest load case of $\sigma_{c,max}$=281.5[MPa] is expected to occur only once in 50 years (extremely low number of cycles), and it is a safe assumption that the fatigue life of the structural steel is satisfactory.

The fatigue analysis of welds of the flush ground monopile is carried out following DNV [35], using the C1 category of S-N curves, as suggested in e.g. Brennan and Tavares [20]. In Table 1, Load Case E-3 can be described as the 50-year ultimate load scenario, while Load Case V represents an estimate of the 1-year highest. Using the thickness correction factor, the representative S-N curve is shown in Fig. 13. Table 13 shows how many cycles the monopile can survive under different stress cycle amplitudes for different load cases described in Table 1.

The simplified procedure arrived at the pile dimensions as follows: 5.2 m diameter and 44.5 long and wall thickness of 59 mm. It is of interest to compare this to the actual foundation dimensions for the

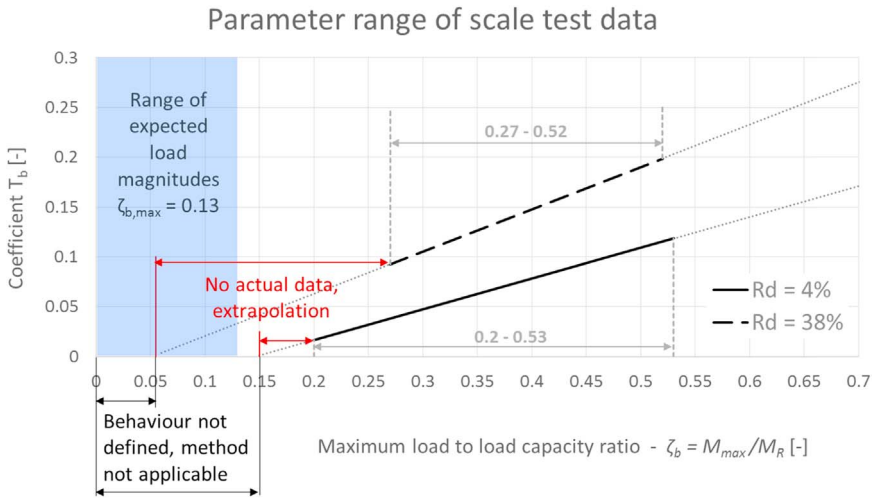

Fig. 12. Range of ζ_b values in the scale tests of Leblanc et al. [52] and values expected for the example case.

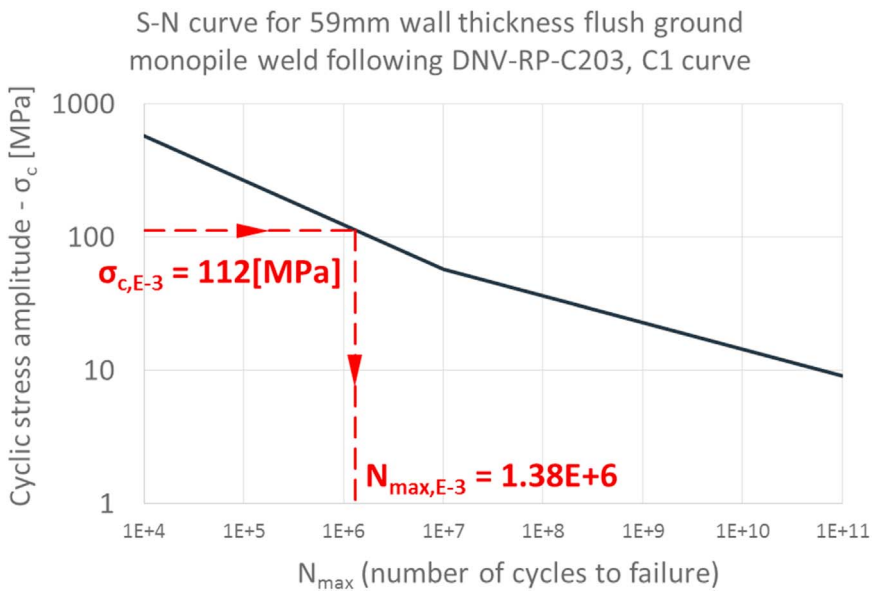

Fig. 13. S-N curve for 59 mm wall thickness flush ground monopile weld following [35].

Table 13
Number of cycles survived at different extreme load scenarios.

Parameter	Normal operation E-1	Extreme wave scenario E-2	Extreme wind scenario E-3	Cut-out wind extreme wave E-4	Wind-wave misalignment E-5
Maximum stress level σm [MPa] as defined in Eq. (93)	162	87	214	123	101
Maximum cyclic stress amplitude σc [MPa] as defined in Eq. (94)	108	86.5	112	92	47.5
Number of cycles the monopile may survive	1.55×10^6	3.02×10^6	1.38×10^6	2.45×10^6	2.63×10^7

London Array wind farm, which is installed in a site with similar conditions to those used in the example. The wind farm comprises of 175 turbines (Siemens SWT-3.6-120) in water depths ranging from 0 to 25 m. The monopile diameters are between 4.7 m and 5.7 m with wall thickness ranging from 44 mm to 87 mm. The piles were hammered up to 40 m into the seabed.

4. Conclusions

Offshore Wind Turbines are dynamically sensitive structures as their natural frequency is close to the forcing frequencies imposed by wind, wave, and mechanical and aerodynamic loads at the frequency of rotation (1P) and blade passing frequency (2P/3P). Therefore the design of foundation needs careful consideration not only from strength consideration but also from stiffness consideration as the deformation (SLS criteria) and dynamics are mainly governed by the stiffness. The load acting on the wind turbine is complex due to variable operation of the rotor during the 20–30 years of design life and uncertainties related to wind and wave misalignment. Load cases have been proposed to obtain foundation design loads. It has been shown that the loads are a functions of the site characteristics (wind, wave and the water depth) and the type of the turbine. The design of monopiles

requires iteration and involves knowledge from many disciplines and therefore a flowchart is presented to capture the interdependency of the parameters and the many disciplines. All the procedure can be implemented through a series of spreadsheets. An example problem is taken to show the application of the simplified method taking an example in similar conditions than those at the London Array wind farm. The resulting pile design is similar to the actual design at the site.

Acknowledgements

The first author is supported by an EPSRC DTP studentship via the University of Bristol.

Appendix A

Table A1 contains the data for the monopile diameters and wall thickness ranges used in Fig. 4.

Table A1
Pile diameters and wall thicknesses of monopiles shown in Fig. 4.

#	Wind farm and turbine	Pile diameter [m]	Wall thickness range [mm]		
1	Lely, Netherlands, A2 turbine	3.2	35	–	35
2	Lely, Netherlands, A3 turbine	3.7	35	–	35
3	Irene Vorrink, Netherlands	3.515	35	–	35
4	Blyth, England, UK	3.5	40	–	40
5	Kentish Flats, England, UK	4.3	45	–	45
6	Barrow, England, UK	4.75	45	–	80
7	Thanet, England, UK	4.7	60	–	60
8	Belwind, Belgium	5	50	–	75
9	Burbo Bank, England, UK	4.7	45	–	75
10	Walney, England, UK	6	60	–	80
11	Gunfleet Sands, England, UK	5	35	–	50
12	London Array, England, UK	4.7	50	–	75
13	Gwynt y Mór, Wales, UK	5	55	–	95
14	Anholt, Denmark	5.35	45	–	65
15	Walney 2, England, UK	6.5	75	–	105
16	Sheringham Shoal, England, UK	5.7	60	–	60
17	Butendiek, Germany	6.5	75	–	90
18	DanTysk, Germany	6	60	–	126
19	Meerwind Ost/Sud, Germany	5.5	50	–	65
20	Northwind, Belgium	5.2	55	–	70
21	Horns Rev, Denmark	4	20	–	50
22	Egmond aan Zee, Netherlands	4.6	40	–	60
23	Gemini, Netherlands	5.5	59	–	73
24	Gemini, Netherlands	7	60	–	85
25	Princess Amalia, Netherlands	4	35	–	79
26	Inner Dowsing, England, UK	4.74	50	–	75
27	Rhyl Flats, Wales, UK	4.72	50	–	75
28	Robin Rigg, Scotland, UK	4.3	50	–	75
29	Teesside, England, UK	4.933	70	–	90

References

[1] Abed Y, Bouzid Djillali Amar, Bhattacharya Subhamoy, Aissa Mohammed H. Static impedance functions for monopiles supporting offshore wind turbines in non-homogeneous soils-emphasis on soil/monopile interface characteristics. Earthq Struct 2016;10(5):1143–79. http://dx.doi.org/10.12989/eas.2016.10.5.1143.

[2] Aldridge TR, Carrington TM, Kee NR. Propagation of pile tip damage during installation. In: Gourvenec , Cassidy , editors. Frontiers in offshore geotechnics. London: Taylor and Francis Group; 2005. p. 823–7, ISBN 0415 39063 X.

[3] 4C Offshore Limited. Offshore Wind Turbine Database. In: 4COffshore.com web page. ⟨http://www.4coffshore.com/windfarms/turbines.aspx⟩; 2016 [accessed 19.03.15].

[4] Achmus M, Kuo Y-S, Abdel-Rahman K. Behavior of monopile foundations under cyclic lateral load. Comput Geotech 2009;36:725–35. http://dx.doi.org/10.1016/j.compgeo.2008.12.003.

[5] Adhikari S, Bhattacharya S. Vibrations of wind-turbines considering soil-structure interaction. Wind Struct 2011;14:85–112.

[6] Adhikari S, Bhattacharya S. Dynamic analysis of wind turbine towers on flexible foundations. Shock Vib 2012;19:37–56.

[7] API . Recommended practice for planning, designing and constructing fixed offshore platforms—working. Stress Des 2005:68–71.

[8] Arany L, Bhattacharya S, Adhikari S, et al. An analytical model to predict the natural frequency of offshore wind turbines on three-spring flexible foundations using two different beam models. Soil Dyn Earthq Eng 2015;74:40–5. http://dx.doi.org/10.1016/j.soildyn.2015.03.007.

[9] Arany L, Bhattacharya S, Adhikari S, et al. An analytical model to predict the natural frequency of offshore wind turbines on three-spring flexible foundations using two different beam models. Soil Dyn Earthq Eng 2015;74:40–5. http://dx.doi.org/10.1016/j.soildyn.2015.03.007.

[10] Arany L, Bhattacharya S, Hogan SJ, Macdonald JHG. Dynamic soil-structure interaction issues of offshore wind turbines. In: Proceedings of the 9th International Conference on Structural Dynamics. EURODYN; 2014. p. 3611–18

[11] Arany L, Bhattacharya S, Macdonald J, Hogan SJ. Simplified critical mudline bending moment spectra of offshore wind turbine support structures. Wind Energy 2015;18:2171–97. http://dx.doi.org/10.1002/we.1812.

[12] Arany L, Bhattacharya S, Macdonald JHG, Hogan SJ. Closed form solution of Eigen frequency of monopile supported offshore wind turbines in deeper waters incorporating stiffness of substructure and SSI. Soil Dyn Earthq Eng 2016;83:18–32. http://dx.doi.org/10.1016/j.soildyn.2015.12.011.

[13] ASTM. E1049-85 Standard practices for cycle counting in fatigue analysis; 2005.

[14] Barber ES. Discussion to paper by S.M. Gleser. ASTM Spec Tech Publ 154; 1953, p. 96–99.

[15] Bhattacharya S. Challenges in Design of Foundations for Offshore Wind Turbines. Eng Technol Ref 2014:1–9, Available at: http://digital-library.theiet.org/content/reference/10.1049/etr.2014.0041.

[16] Bhattacharya S, Cox JA, Lombardi D, Wood Muir Wood DM. Dynamics of offshore wind turbines supported on two foundations. Proc ICE - Geotech Eng 2013;166:159–69. http://dx.doi.org/10.1680/geng.11.00015.

[17] Bhattacharya S, Nikitas N, Garnsey J, et al. Observed dynamic soil–structure interaction in scale testing of offshore wind turbine foundations. Soil Dyn Earthq Eng 2013;54:47–60. http://dx.doi.org/10.1016/j.soildyn.2013.07.012.

[18] Bhattacharya S, Carrington TM, Aldridge TR. Buckling considerations in pile design. In: Gourvenec S, Cassidy M, editors. Front Offshore Geotech. London, UK: Taylor & Francis Group; 2005. p. 815–22, ISFOG 2005.

[19] Bouzid DA, Bhattacharya S, Dash SR. Winkler Springs (p-y curves) for pile design from stress-strain of soils: FE assessment of scaling coefficients using the mobilized strength design concept. Geomech Eng 2013;5(5):379–99. http://dx.doi.org/10.12989/gae.2013.5.5.379.

[20] Brennan F, Tavares I. Fatigue design of offshore steel monopile wind substructures. Inst Civ Eng 2014;167:1–7.

[21] Broms BB. Lateral resistance of pile in cohesionless soils. J Soil Mech Found Div ASCE 1964;90:123–56.

[22] Burton T, Jenkins N, Sharpe D, Bossanyi E. Wind energy handbook. Chichester, West Sussex, England: John Wiley & Sons, Ltd; 2001.

[23] Burton T, Sharpe D, Jenkins N, Bossanyi E. Wind energy handbook, 2nd ed. 2011; 2011. http://dx.doi.org/10.1002/0470846062.

[24] Byrne BW, McAdam R, Burd H, Houlsby GT, Martin C, et al. New design methods for large diameter piles under lateral loading for offshore wind applications. Front Offshore Geotech III, CRC Press; 2015, p. 705–10. http://dx.doi.org/10.1201/b18442-96

[25] Byrne BW, Houlsby GT, Leblanc C. Response of stiff piles to random two-way lateral loading. Géotechnique 2010;60:715–21. http://dx.doi.org/10.1680/geot.09.T.011.

[26] Byrne BW, McAdam RA, Burd HJ, et al. Field testing of large diameter piles under lateral loading for offshore wind applications. In: Proceedings of the XVI ECSMGE geotechnical engineering for infrastructure and development; 2015. p. 1255–60. http://dx.doi.org/10.1680.60678

[27] Camp TR, Morris MJ, van Rooij R, van der Tempel J, Zaaijer M, Henderson A, et al. Design methods for offshore wind turbines at exposed sites (final report of the OWTES project EU Joule III project JOR3-CT98-0284). Bristol; 2004

[28] Carter J, Kulhawy F. Analysis of laterally loaded shafts in rock. J Geotech Eng 1992;118:839–55.

[29] Cox J a, O'Loughlin CD, Cassidy M, et al. Centrifuge study on the cyclic performance of caissons in sand. Int. J Phys Model Geotech 2014;14:99–115. http://dx.doi.org/10.1680/ijpmg.14.00016.

[30] Cuéllar P. Pile foundations for offshore wind turbines: numerical and experimental investigations on the behaviour under short-term and long-term cyclic loading. Technischen Universität, Berlin; 2011

[31] Damgaard M, Zania V, Andersen L, Ibsen LB. Effects of soil–structure interaction on real time dynamic response of offshore wind turbines on monopiles. Eng Struct 2014;75:388–401. http://dx.doi.org/10.1016/j.engstruct.2014.06.006.

[32] Davisson MT. Lateral load capacity of piles. Highw Res Rec 1970:104–12.

[33] Davisson MT, Salley JR. Model study of laterally loaded piles. J Soil Mech Found Div 1970;96:1605–27.

[34] DNV. Offshore Standard DNV-OS-J101 Design of offshore wind turbine structures. Høvik, Norway; 2014.
[35] DNV. DNV-RP-C203- Fatigue design of offshore steel structures. Recomm Pract DNV-RPC203 126; 2005.
[36] DNV. Recommended Practice DNV-RP-C205 - Environmental conditions and environmental loads; 2010.
[37] European Committee for Standardization. Eurocode 8: Design of Structures for earthquake resistance - Part 5: Foundations, retaining structures and geotechnical aspects; 2003.
[38] Frohboese P, Schmuck C. Thrust coefficients used for estimation of wake effects for fatigue load calculation. In: Proceedings of the European Wind Energy Conference, Warsaw, Poland; 2010. p. 1–10
[39] Gazetas G. Seismic response of end-bearing single piles. Int J Soil Dyn Earthq Eng 1984;3:82–93. http://dx.doi.org/10.1016/0261-7277(84)90003-2.
[40] GermanischerLloyd. Guideline for the certification of offshore wind turbines. Uetersen, Germany; 2005.
[41] Hald T, Mørch C, Jensen L, Leblanc C, Ahle K. Revisiting monopile design using p-y curves Results from full scale measurements on Horns Review.In: Proceedings of the European Wind Energy Conference; 2009
[42] Hettler A. Verschiebungen starrer und elastischer Gründungskörper in Sand bei monotoner und zyklischer Belastung. Univ. Fridericiana, Karlsruhe; 1981
[43] Higgins W, Basu D. Fourier finite element analysis of laterally loaded piles in elastic media – Internal Geotechnical Report 2011–1. Storrs, Connecticut; 2011
[44] IEC. International Standard IEC-61400-1 wind turbines – Part 1: design requirements, 3rd ed.; 2005.
[45] IEC. International Standard IEC 61400-3 wind turbines – Part 3: design requirements for offshore wind turbines, 1.0 ed. International Electrotechnical Commission (IEC); 2009.
[46] IEC. International Standard IEC-61400-1 Amendment 1 – wind turbines – Part 1: design requirements, 3rd ed.; 2009.
[47] Kallehave D, Thilsted CL. Modification of the API p-y formulation of initial stiffness of sand. Offshore Site Investigation Geotechnique Integrated Geotechnologies – Present Futur; 2012
[48] Klinkvort RT, Leth CT, Hededal O. Centrifuge modelling of a laterally cyclic loaded pile. In: Proceedings of the 7th international conference of physical modelling in geotechnics; 2010. p. 959–64
[49] Kucharczyk P, Rizos A, Münstermann S, Bleck W. Estimation of the endurance fatigue limit for structural steel in load increasing tests at low temperature. Fatigue Fract Eng Mater Struct 2012;35:628–37. http://dx.doi.org/10.1111/j.1460-2695.2011.01656.x.
[50] Kühn M. Soft or stiff: a fundamental question for designers of offshore wind energy converters. In: Proceedings of the European wind energy conference. EWEC'97; 1997
[51] Kuo Y-S, Achmus M, Abdel-Rahman K. Minimum embedded length of cyclic horizontally loaded monopiles. J Geotech Geoenviron Eng 2012;138:357–63. http://dx.doi.org/10.1061/(ASCE)GT.1943-5606.0000602.
[52] Leblanc C, Houlsby GT, Byrne BW. Response of stiff piles in sand to long-term cyclic lateral loading. Géotechnique 2010;60:79–90. http://dx.doi.org/10.1680/geot.7.00196.
[53] Li Z, Haigh SK, Bolton MD. Centrifuge modelling of mono-pile under cyclic lateral loads. In: Proceedings of the 7th internationa conference of physical modelling in geotechnics 2 ,vol. 2; 2010. p. 965–70
[54] Lin S-S, Liao J-C. Permanent strains of piles in sand due to cyclic lateral loads. J Geotech Geoenviron Eng 1999;125:798–802.
[55] Lindoe Offshore Renewables Center. Offshore Wind Farm Knowledge Base. In: lorc.dk web page. ⟨http://www.lorc.dk/knowledge⟩ ; 2011. [accessed 19.03.15].
[56] Little RL, Briaud J-L. Full scale cyclic lateral load tests on six single piles in sand (No. TAMU-RR-5640). College Station, Texas; 1988
[57] Lombardi D, Bhattacharya S, Muir Wood D. Dynamic soil–structure interaction of monopile supported wind turbines in cohesive soil. Soil Dyn Earthq Eng 2013;49:165–80. http://dx.doi.org/10.1016/j.soildyn.2013.01.015.
[58] Long JH, Vanneste G. Effects of cyclic lateral loads on piles in sand. J Geotech Eng 1994;120:225–44.
[59] Matlock H. Correlations for design of laterally loaded piles in soft clay. In: Proceedings of the Second Annual Offshore Technology Conference; 1970
[60] Matlock H, Foo DHC, Bryant LM. Simulation of lateral pile behavior under earthquake motion. In: Proceedings of the ASCE special conference on earthquake engineering soil dynamics. American Society of Civil Engineers, 19–21 June, Pasadena, California; 1978. p. 600–19
[61] Matsuishi M, Endo T. Fatigue of metals subjected to varying stress. Japan Soc Mech Eng 1968.
[62] Miner MA. Cumulative damage in fatigue. Am Soc Mech Eng – J Appl Mech 1945;12:159–64.
[63] Morison JR, Johnson JW, Schaaf SA. The force exerted by surface waves on piles. J Pet Technol 1950;2:149–54, 10.2118/950149-G.
[64] O'Neill MW, Murchinson JM. An Evaluation of p-y relationships in sands; Houston, TX, US: University of Houston; 1983
[65] Pender MJ. Aseismic pile foundation design analysis. Bull N Z Natl Soc Earthq Eng 1993;26:49–161.
[66] Poulos H, Davis E. Pile foundation analysis and design. Rainbow-Bridge Book Co.; 1980.
[67] Prakash S. Behaviour of pile groups subjected to lateral loads. Urbana-Champaign: University of Illinois; 1962.
[68] Randolph M, Gourvenec MRS. Offshore Geotechnical Engineering. New York, USA: Spon Press (Taylor & Francis); 2011
[69] Randolph MF. The response of flexible piles to lateral loading. Géotechnique 1981;31:247–59.
[70] Reese LC, Cox WR, Koop FD. Field testing and analysis of laterally loaded piles in stiff clay. In: Proceedings of the seventh annual offshore technology conference; 1975
[71] Reese LC, Cox WR, Koop FD. Analysis of Laterally Loaded Piles in Sand. Pap. No. 2080. In: Proceedings of the Sixth Annual Offshore Technology Conference; 1974
[72] Shadlou M, Bhattacharya S. Dynamic stiffness of monopiles supporting offshore wind turbine generators. Soil Dyn Earthq Eng 2016:15–32, http://dx.doi.org/10.1016/j.soildyn.2016.04.002.
[73] Swane IC, Poulos H. A theoretical study of the cyclic shakedown of laterally loaded piles. Sydney; 1982
[74] Terzaghi K. Evaluation of coefficient of subgrade reaction. Geotech, London 5; 1955, p. 41–50
[75] Verdure L, Garnier J, Levacher D. Lateral cyclic loading of single piles in sand. Int J Phys Model Geotech 2003;3:17–28.
[76] Williams MO. Wave mapping in UK waters. Yarmouth, Isle of Wight; 2008
[77] Winkler E. Die Lehre Von der Elasticitaet und Festigkeit. H. Dominicus, Prag; 1867
[78] Zaaijer MB. Foundation modelling to assess dynamic behaviour of offshore wind turbines. Appl Ocean Res 2006;28:45–57. http://dx.doi.org/10.1016/j.apor.2006.03.004.
[79] Zania V. Natural vibration frequency and damping of slender structures founded on monopiles. Soil Dyn Earthq Eng 2014;59:8–20. http://dx.doi.org/10.1016/j.soildyn.2014.01.007.
[80] Zdravkovic L, Taborda DMG. Numerical modelling of large diameter piles under lateral loading for offshore wind applications. In: Meyer , editor. Frontiers in offshore geotechnics III. London: Taylor & Francis Group; 2015. p. 759–64.
[81] Zhu B, Byrne B, Houlsby G. Long-term lateral cyclic response of suction caisson foundation in sand. J Geotech Geoenviron Eng 2012:73–83. http://dx.doi.org/10.1061/(ASCE)GT.1943-5606.0000738.